IEEE Access
Multidisciplinary ⋮ Rapid Review ⋮ Open Access Journal

Received November 29, 2021, accepted January 11, 2022, date of publication January 13, 2022, date of current version January 20, 2022.

Digital Object Identifier 10.1109/ACCESS.2022.3142742

Coot Bird Algorithms-Based Tuning PI Controller for Optimal Microgrid Autonomous Operation

AHMED MOREAB HUSSIEN[1], RANIA A. TURKY[1], ABDULAZIZ ALKUHAYLI[2], (Member, IEEE), HANY M. HASANIEN[3], (Senior Member, IEEE), MARCOS TOSTADO-VÉLIZ[4], FRANCISCO JURADO[4], (Senior Member, IEEE), AND RAMESH C. BANSAL[5,6], (Senior Member, IEEE)

[1]Electrical Engineering Department, Faculty of Engineering and Technology, Future University in Egypt, Cairo 11835, Egypt
[2]Electrical Engineering Department, College of Engineering, King Saud University, Riyadh 11421, Saudi Arabia
[3]Electrical Power and Machines Department, Faculty of Engineering, Ain Shams University, Cairo 11517, Egypt
[4]Department of Electrical Engineering, Superior Polytechnic School of Linares, University of Jaén, 23700 Linares, Spain
[5]Electrical Engineering Department, University of Sharjah, Sharjah, United Arab Emirates
[6]Department of Electric, Electronic and Computer Engineering, University of Pretoria, Pretoria 0028, South Africa

Corresponding author: Ahmed Moreab Hussien (ahmed.moreab@fue.edu.eg)

This work was supported by the Researchers Supporting Project, King Saud University, Riyadh, Saudi Arabia, under Grant RSP-2021/258.

ABSTRACT This paper develops a novel methodology for optimal control of islanded microgrids (MGs) based on the coot bird metaheuristic optimizer (CBMO). To this end, the optimum gains for the PI controller are found using the CBMO under a multi-objective optimization framework. The Response Surface Methodology (RSM) is incorporated into the developed procedure to achieve a compromise solution among the different objectives. To prove the effectiveness of the new proposal, a benchmark MG is tested under various scenarios, 1) isolate the system from the grid (autonomous mode), 2) islanded system exposure to load changes, and 3) islanded system exposure to a 3 phase fault. Extensive simulations are performed to validate the new method taking conventional data from PSCAD/EMTDC software. The validity of the suggested optimizer is proved by comparing its results with that achieved using the LMSRE-based adaptive control, sunflower optimization algorithm (SFO), Ziegler-Nichols method and the particle swarm optimization (PSO) techniques. The article shows the superiority of the suggested CBMO over the LMSRE-based adaptive control, SFO, Ziegler-Nichols and the PSO techniques in the transient responses of the system.

INDEX TERMS Distributed generators, sunflower optimization algorithm, microgrid, renewable energy, coot bird metaheuristic optimizer.

I. INTRODUCTION

A. LITERATURE SURVA

Because of the ever-increasing demand for electric energy and growing environmental concern about pollution and greenhouse gas emissions, the energy market is increasingly embracing distributed energy resources (DERs) such as fuel cells, photovoltaic (PV) systems, micro-turbines, wind farms, etc. [1]–[4]. Most of the DER-based distributed generators (DGs) are connected to the electric grid using voltage source inverters (VSIs) [5]. These inverter-based DGs have entirely different physical properties than traditional synchronous generators (SGs). As a result, various control techniques for VSIs based on DGs are necessary for desired control action. The SG, for example, has a high inertia because of its huge spinning mass, which contributes to grid stability by sustaining the grid frequency. The lack of inertia and rotational mass in DGs creates technical difficulties, such as the requirement for storage units and suitable regulatory systems to maintain grid stability. As a result, the concept of the microgrid (MG) is being promoted.

The MG is a controlled structure made up of numerous DG units, loads, and storage facilities that are all tied to a local network. The MG can be operated in off-grid or in grid-connected modes [6]. MGs are frequently located near loads to reduce the transmission losses, offer reliable power supply and permit several RESs to collaborate in a distributed form, leading to greater supply security. The grid sets the operating voltage and frequency in the grid-connected mode. On the other hand, the VSI has to maintain these functions

The associate editor coordinating the review of this manuscript and approving it for publication was Emanuele Crisostomi.

in islanded mode [7]–[9]. In this regard, the control of VSI interfaces becomes more difficult [10], [11].

Advanced control systems are therefore employed in off-grid mode to guarantee applicable and reliable operation. These control systems are grouped into 3 classes, droop-based control, centralized control, and multivariable and servomechanism (MVAS) techniques. Droop control is utilized in relying on SG droop characteristics, to offer peer-to-peer control and plug-and-play features by independently managing the power output of separate DG units without the need for interaction or coordination among DGs. A wireless control strategy concentrated on P-Q droop management has been recommended [12]. In [13], a complete decentralized method relying on dual-frequency-droop control is offered. The capacity of autonomously regulate distributed units without interaction among them is one of the advantages of utilizing droop-based control. This scheme outperforms other power-sharing and MG frequency regulation methods in terms of robustness and consistency. But, for low voltage MGs with resistor line impedance, droop control efficiency is strongly impacted by line impedance, leading to power couplings [14]. The virtual vector transformation technique has been enhanced [15] to evade power coupling, but it reduces the stability of the system. On the contrary, centralized control techniques need high bandwidth interconnections and any breakdown of such links might result in a microgrid failure. In [16], A centralized control system for DC MG based on autonomous communication has been designed and deployed. To end with, a novel approach for developing multivariable resilient servomechanism systems for multi-input multi-output open-loop stable systems has been suggested in [17]. Unfortunately, its great complexity is a burden.

For nonlinear problems, it is found that the most frequently applied controller is the proportional-integral (PI) scheme due to its great stability margin. Unfortunately, it struggles with parameter fluctuation sensitivity and network nonlinearity. As a result, determining the appropriate PI controller settings in this nonlinear system is a significant problem.

B. RESEARCH GAP AND MOTIVATION

In the past few years, extensive research has been done to design the optimum controller for MG systems to assure successful performance. In this regard, PI controllers maintain the voltage source converter (VSC) voltage with the aid of a d-q frame [18]. PI controllers are regulated using simple approaches like the Zigler Nicholas [19] method when assuming linearity of the system. Conversely, the PI controller creates a saturation outcome, decreasing the control stability margin as a result of a more significant phase lagging. Controllers are frequently responsive to changes in parameters and operating conditions [20]. In [21], a distributed PI controller to regulate a hybrid power system P&Q is presented. Subsequent, numerous optimization techniques, including particle swarm optimization (PSO) [22], Heap optimization algorithm (HOA) [23], genetic algorithm (GA) [24], sunflower optimization algorithm (SFO) [25], hybrid firefly and particle swarm optimization technique [26], Salp swarm algorithm [27], hybrid GWO-PSO optimization technique [28], hybrid cuckoo search algorithm and grey wolf optimizer (CSA–GWO) [29], equilibrium optimization algorithm (EO) [30], and Whale Optimization Algorithm (WOA) [31], have been used in the MG to enhance decentralized controllers. As reported in [32], these approaches have however advantages and disadvantages, being still so far to get a universal framework for MG control.

This paper contributes to this pool by developing a novel methodology for optimal control of islanded MGs based on the coot bird metaheuristic optimizer (CBMO). In this research, this optimizer is used in a PI controller optimal control scheme with various PI controller gains to enhance the efficacy of the islanding microgrid operation. Furthermore, the Response Surface Methodology (RSM) is considered to attain a compromise solution among objectives under a multi-objective optimization paradigm. To validate the new proposal, various simulations are carried out to show the superiority of the suggested CBMO in the transient responses of the system over Ziegler-Nichols and some other optimization techniques, such as the LMSRE-based adaptive control, SFO and the PSO techniques.

C. CONTRIBUTION AND PAPER BOD

To cover the gaps previously exposed, this article contributes with:

1) Developing a novel methodology based on CBMO to adjust PI controllers to improve the efficiency of the MG system,
2) Evaluate the reliability of the suggested optimizer through experiment the MG under various operating modes, i) cut the system off the grid (autonomous mode), ii) islanded system interrupted by a load changes, and iii) islanded system interrupted by a 3 phase fault,
3) Proving the validity of the offered optimizer through comparing its results with that achieved using the LMSRE-based adaptive control, SFO and, Ziegler-Nichols the PSO techniques.

The leftover sectors of the article are ordered in this way. Sector II demonstrates the MG demonstrating. Sector III explains the control plan. Sector IV shows the design procedures. Sectot V shows the modelling stage of the Response Surface Methodology (RSM), SFO, LMSRE adaptive control, Ziegler-Nichols and the CBMO. Sector VI introduces the simulation results and discussion. Lastly, the conclusion is introduced in Sectot VII.

II. MG DEMONSTRATING

Fig. 1 depicts a single line diagram of a benchmark MG, which is mainly divided into three DGs linked together via transmission lines. The utility grid is connected to the DGs via a point of common coupling (PCC) through transmission lines. The single DG is made up of a DC supply connected to pulse width modulation (PWM) (2 levels), which is linked to a delta-star transformer via a filter to avoid power quality issues. To represent the local load, RLC load is inserted after the Δ - Y transformer. The MG information is listed in Table 1.

TABLE 1. MG data.

Transformer data		Δ/Y = 0.6/13.8 KV
Load data	Load 1	C_l= 50μF, R_{l1}=9Ω, R_{l2}=150Ω, L_l=0.6 H
	Load 2	C_2= 42μF, R_{22}=5Ω, R_{l2}=75Ω, L_2=0.4 H
	Load 3	C_3= 33μF, R_{33}=20Ω, R_{l2}=50Ω, L_3=1.5 H
Transmission Line parameters	TL1	R_{TL1}= 0.7 Ω, L_{TL1} = 0.5 mH
	TL2	R_{TL2} = 1.5 Ω, L_{TL2} = 0.9 mH
Filter data		R_f = 1.5 mΩ, X_f = 0.5 mH
Grid parameters		V = 13.8 KV, R_g=0.2 Ω, L_g=0.3 mH

The study MG can be operated either in grid-connected or in stand-alone mode. The DG operates in power control mode when connected to the grid. It is worthy to note that the grid sustains the voltage and frequency. Conversely, in the off-grid mode, the DG is in charge of balancing demands and generation. Moreover, it adjusts the voltage and frequency to sustain them inside acceptable ranges. This study focuses on improving the MG under off-grid operating mode by employing the cascaded control method, which is detailed in the following sector.

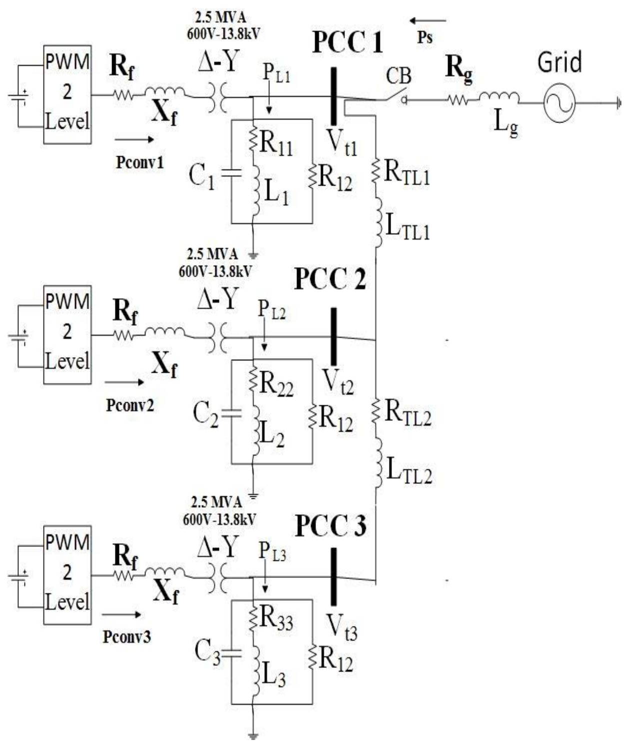

FIGURE 1. Single line diagram of a benchmark MG.

III. CONTROL PLAN

In each DG, the cascaded control scheme is used to stabilize the voltage at the PCC. The reference voltages ($V_{conv\_a}{}^*$, $V_{conv\_b}{}^*$, $V_{conv\_c}{}^*$) are achieved by the Inverse Clarke Transformation of the d-q reference voltages ($V_{conv\_d}{}^*$, $V_{conv\_q}{}^*$) and the transformation angle (θ_{PLL}). $V_{conv\_d}{}^*$ and $V_{conv\_q}{}^*$ are given with the aid of the 4 PI controllers as seen in Fig. 2. θ_{PLL} is taken from the phase-locked loop by taking the data of the voltages of the grid in the inputs. The inverter switches pulses are achieved with the aid of the comparator that compares a 1980 Hz (60 HZ multiples) triangular signal and the reference voltages ($V_{conv\_a}{}^*$, $V_{conv\_b}{}^*$, $V_{conv\_c}{}^*$).

The gains of the 4 PI controllers are determined using the CBMO method and other optimization techniques. Section IV goes into further depth on this.

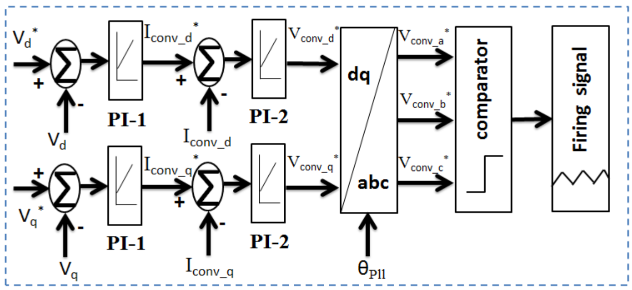

FIGURE 2. Control system for off-grid mode.

IV. DESIGN PROCEDURES

A. SELECTION OF VARIABLES

In this article, six PI controllers are employed in 3 DGs, two in for each DG, where:

- $PI_{1.1}$ and $PI_{1.2}$ are the PI controllers utilized in DG_1,
- $PI_{2.1}$ and $PI_{2.2}$ are the PI controllers utilized in DG_2 and
- $PI_{3.1}$ and $PI_{3.2}$ are the PI controllers utilized in DG_3

The proportional gain (KP) and integral time constants (TI) are the gains for the PI controllers in this research where:

- Y_1 is the KP of the $PI_{1.1}$ in DG_1,
- Y_2 is the TI of the $PI_{1.1}$ in DG_1,
- Y_3 is the KP of the $PI_{1.2}$ in DG_1,
- Y_4 is the TI of the $PI_{1.2}$ in DG_1,
- Y_5 is the KP of the $PI_{2.1}$ in DG_2,
- Y_6 is the TI of the $PI_{2.1}$ in DG_2,
- Y_7 is the KP of the $PI_{2.2}$ in DG_2,
- Y_8 is the TI of the $PI_{2.2}$ in DG_2,
- Y_9 is the KP of the $PI_{3.1}$ in DG_3,
- Y_{10} is the TI of the $PI_{3.1}$ in DG_3,
- Y_{11} is the KP of the $PI_{3.2}$ in DG_3 and
- Y_{12} is the TI of the $PI_{3.2}$ in DG_3.

In this article, three levels are utilized for the controllers' variables, which are summarized in Table 2.

- Level -1 is the minimum safe value,
- Level 0 is the average value between Level 1 and -1 and
- Level 1 is the maximum safe value.

TABLE 2. RSM levels.

Design variable level	Level (-1)	Level (0)	Level (1)
Y_1	2	4.75	7.5
Y_2	0.0009	0.01045	0.02
Y_3	1.6	2.3	3
Y_4	0.05	1.525	3
Y_5	1.5	4.25	7
Y_6	0.0009	0.00795	0.015
Y_7	1.4	1.95	2.5
Y_8	0.05	1.425	2.8
Y_9	1	3.75	6.5
Y_{10}	0.0009	0.00545	0.01
Y_{11}	1.2	1.65	2.1
Y_{12}	0.05	1.275	2.5

B. PSCAD/EMTDC PROGRAM

PSCAD software is used to simulate the MG system. The information extracted from these simulations in various scenarios is utilized to be the inputs of the RSM.

TABLE 3. The input weights.

Weight (Wt)	location		Value
Wt_1	DG1	MPUS	0.2
Wt_2		MPOS	0.2
Wt_3		T_{set}	0.075
Wt_4		E_{ss}	0.03
Wt_5	DG2	MPUS	0.125
Wt_6		MPOS	0.125
Wt_7		T_{set}	0.04
Wt_8		E_{ss}	0.02
Wt_9	DG3	MPUS	0.075
Wt_{10}		MPOS	0.075
Wt_{11}		T_{set}	0.025
Wt_{12}		E_{ss}	0.01

C. THE RSM & MINITAB SOFTWARE

The RSM is a mathematical procedure that empirically creates models by utilizing a good statistical approach to detect correlations between control and dynamic behaviour [33]. The steady-state error (E_{ss}), maximum percentage under/overshoots (MPUS/MPOS), and settling time (T_{set}) of the reference voltage are the RSM input data which are extracted from PSCAD and presented in Table 12, Table 13, and Table 14 in the Appendix. The RSM is constructed with the aid of MINITAB software.

The multi-objective function for this system is defined by the minimization of the MPOS (N1), MPUS (N2), T_{set} (N3), and E_{ss} (N4) for the given scenarios. Eq. (1) depicts the second order polynomial RSM model.

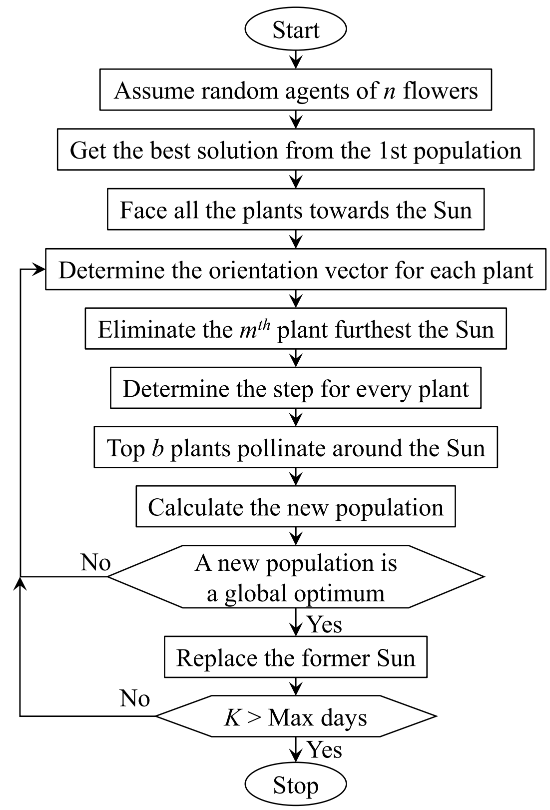

FIGURE 3. Flowchart of SFO algorithm.

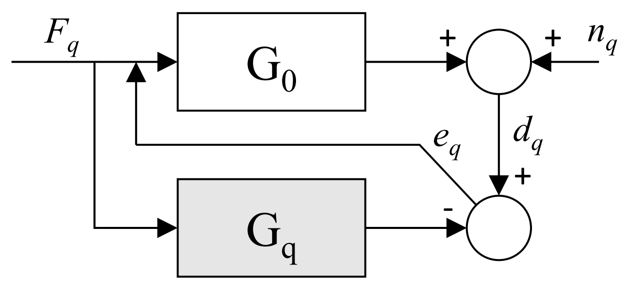

FIGURE 4. System prototypal of FIR filter.

$$
\begin{aligned}
N_i = {} & M_1 + M_2Y_1 + M_3Y_2 + M_4Y_3 + M_5Y_4 \\
& + M_6Y_1^2 + M_7Y_2^2 + M_8Y_3^2 + M_9Y_4^2 + M_{10}Y_1Y_2 \\
& + M_{11}Y_1Y_3 + M_{12}Y_1Y_4 + M_{13}Y_2Y_3 + M_{14}Y_2Y_4 \\
& + M_{15}Y_3Y_4 \qquad (1)
\end{aligned}
$$

where i = 1, 2, 3, 4, and $M_1, M_2 \ldots, M_{15}$ are the computed RSM coefficients for the scenarios are reported in Table 15, Table 16, and Table 17 in the Appendix.

V. OPTIMIZATION STAGE

Eq. (1) relies on the weighting technique [34] is utilized as an input to the CBMO, SFO, and PSO techniques to achieve the optimum PI gains that reduce the transients. The weights utilized in the multi-objective function are listed in Table 3.

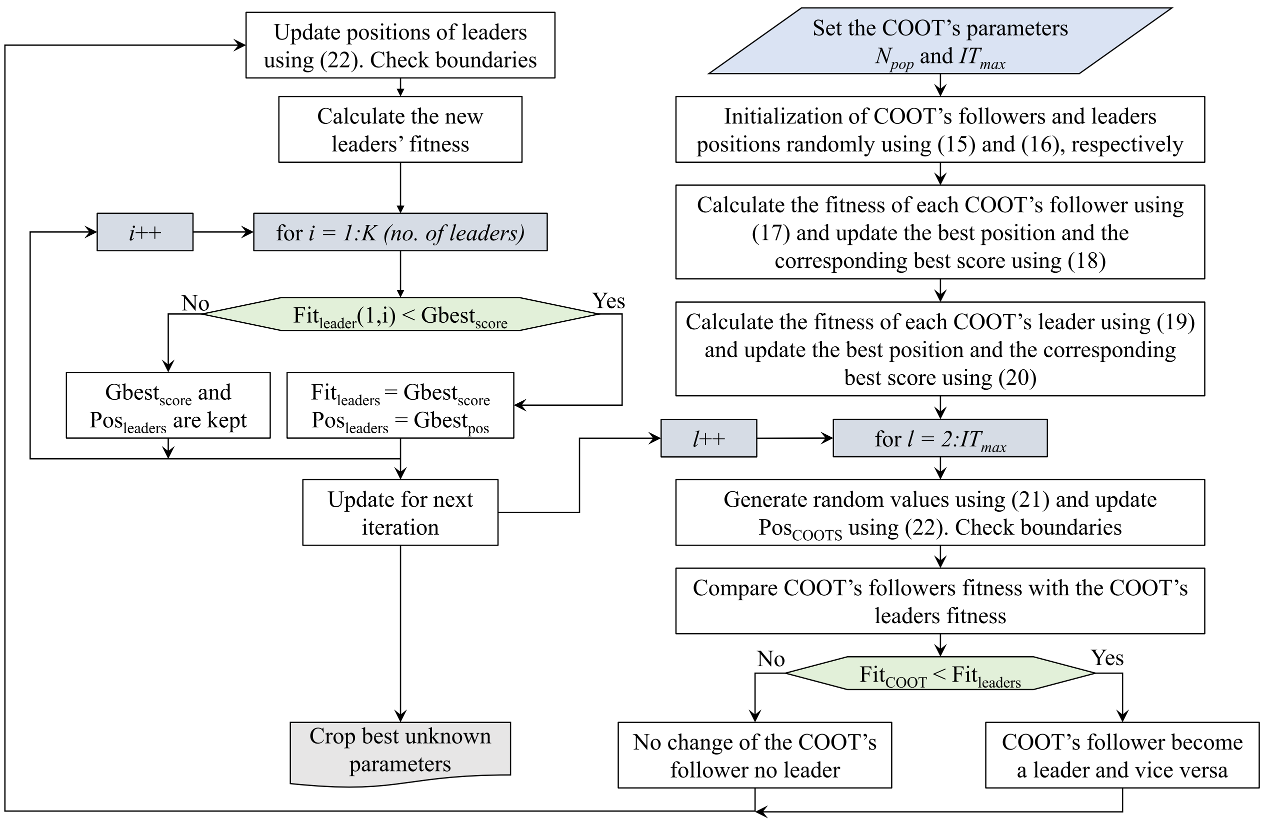

FIGURE 5. Flowchart of CMBO algorithm.

A. THE SFO ALGORITHM

The advancement of soft computing capability is the primary impetus for using SFO in the optimization of various issues. The SFO is a natural-motivated heuristic method. Its basic concept is to simulate the configuration of sunflowers to gather sunlight [25]. Daily basis, the sunflower pattern is replayed, started in the sunrise tracking the sunlight and ending in the sundown. The sunflower back into its original place in the evening, waiting for the sun to appear. Each sunflower is thought to have only one pollen gamete. Radiation from the inverse square rule is critical in this case. Because sunflowers absorb a tremendous quantity of energy from the sun relative to those further away. The sunflowers near to the sun tilt toward calm in this location [25]. Eq. (2) indicates the heat absorbed by each population.

$$H_s = \frac{W}{4\pi r_s^2} \tag{2}$$

where W is the power source, and r_s denotes the distance between the most frequent best and population i. Eq. (3) illustrates the movement of sunflowers [13], while the movement of sunflowers in the direction of "m" is given by Eq. (4).

$$\vec{m}_i = \frac{Z^* - Z_i}{||Z^* - Z_i||}, \quad i = 1, 2, \ldots, n_p \tag{3}$$

$$d_i = A \times P_i (Z_i + Z_{i-1}) \times ||Z_i + Z_{i-1}|| \tag{4}$$

where z is the population, z* is the best population, np is the population number, A is a constant that characterizes the "inertial" motion of the sunflowers and $P_i(||z_i + z_{i-1}||)$ is the pollination possibility. Eq. (5) specifies the constraint of these phases:

$$R_{max} = \frac{||Z_{max} - Z_{min}||}{2 \times n_p} \tag{5}$$

where Z_{max} and Z_{min} are the minimum and maximum boundaries, respectively. The following plant is defined as follows.

$$\vec{Z}_{i+1} = \vec{Z}_i + d_i \times \vec{m}_i \tag{6}$$

For the sake of clarity, the overall procedure of SFO is summarized in the flowchart of Fig. 3, while the results for this algorithm were taken from [6].

B. LMSRE ALGORITHM

The adaptive filtering algorithms (AFAs) are normally utilized to discover the impulse response weight vector (G_0) filter [35], as represented in Fig. 4. The input Fq is implemented as a Gaussian noise Nq going over FIR filter. Consequently, it depends on the error e_q.

The AFAs are iterated using the steepest descent technique, as indicated in Eq (7).

$$G_{q+1} = G_q - \mu \nabla_G j\left(G_q\right) \tag{7}$$

TABLE 4. The initial LMSRE PI gains.

controller	$PI_{1.1}$	$PI_{1.2}$	$PI_{2.1}$	$PI_{2.2}$	$PI_{3.1}$	$PI_{3.2}$
initial k_p	5.5	3	5.5	3	5.5	3
initial T_i	0.003	0.3	0.003	0.3	0.003	0.3

TABLE 5. Rules for PI gains based on ziegler–nichols technique [36].

Controller type	K_P	T_I	Kd
P	0.5 K_{cr}	Inf.	0
PI	0.45 K_{cr}	(1/1.2) P_{cr}	0
PID	0.6 K_{cr}	0.5 P_{cr}	0.125 P_{cr}

TABLE 6. The ziegler-nichols critical gains (kcr) and critical periods (Pcr) for the DGs for scenario1.

	Critical gains (k_{cr})	Critical periods (P_{cr})	PI gains	
$PI_{1.1}$	7.5	0.0048	Y_1	3.375
			Y_2	0.004
$PI_{2.1}$	3	1.2	Y_3	1.35
			Y_4	1
$PI_{2.1}$	7	0.00456	Y_5	3.15
			Y_6	0.0038
$PI_{2.2}$	2.5	1.1856	Y_7	1.125
			Y_8	0.988
$PI_{3.1}$	6.5	0.00432	Y_9	2.925
			Y_{10}	0.0036
$PI_{3.2}$	2.1	1.1532	Y_{11}	0.945
			Y_{12}	0.961

where q is the iteration number and W_q expresses the estimated vector of the weight. Next, the gradient of the cost function is achieved from Eq. (8).

$$\nabla_{Gj}\left(G_q\right)=\text{sign}\left(e_q\right)\cdot\left(-F_q\right)-\left[\frac{\exp\left(-\left|e_q\right|\right)}{\sqrt{1}+\exp(-\left|e_q\right|)}\right] \tag{8}$$

By substituting Eq. (7) into Eq. (8) one obtains

$$G_{q+1} = G_q - \mu_q\beta_q\text{sign}\left(e_q\right)\cdot F_q \tag{9}$$

where μ_q is set to bound the errors. For instance, for the giant error, μ_q must be large for quick convergence. Conversely, for a minor error, μ_q needs to be reduced. So, β_q diverges from [0, 1], and is reduced for small errors and vice versa. Therefore, μ_q diverges proportionately to the β_q which stated in eq.(10).

$$\mu_q = \mu\beta_q^{\alpha-1} \tag{10}$$

where μ and α are in control of deviation of μ_q. Then, replacing Eq. (9) into Eq. (10) yields

$$G_{q+1} = G_q - \mu\beta_q^{\alpha}\text{sign}\left(e_q\right)\cdot F_q \tag{11}$$

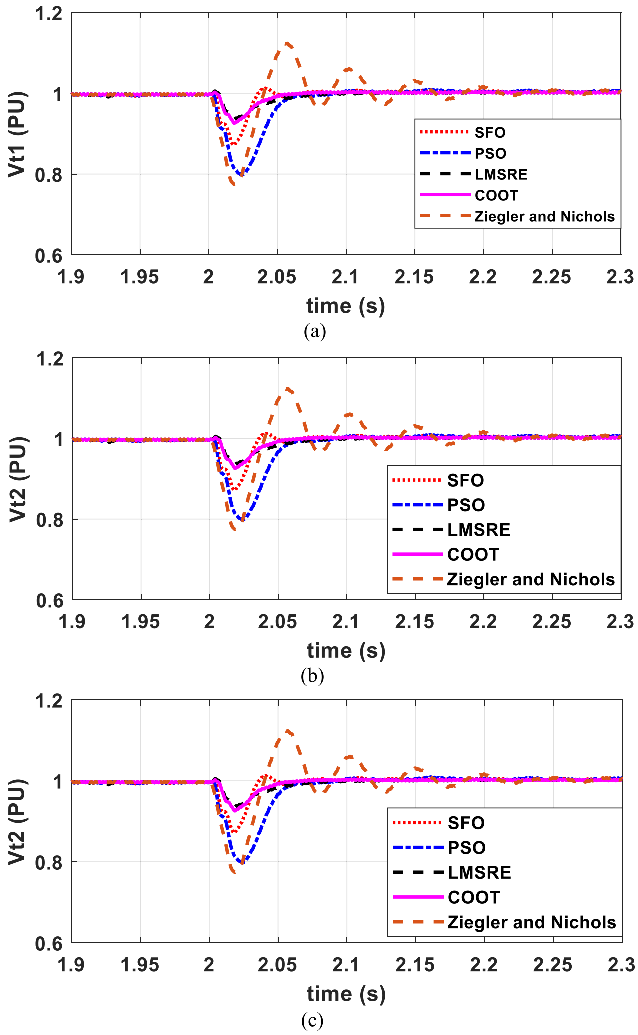

FIGURE 6. The results of CBMO, SFO, PSO, ziegler-nichols and LMSRE for scenario1. (a) Reference voltage of DG 1. (b) Reference voltage of DG 2. (c) Reference voltage of DG 3.

The LMSRE method is used to modify the PI Controller methods that rely on eq (11). The following are the adjusted PI parameters:

$$k_{p(q+1)} = k_{p(q)}+\Delta k_{p(q)} \tag{12}$$

$$T_{i(q+1)} = T_{i(q)}+\Delta T_{i(q)} \tag{13}$$

$$\Delta k_{p(q)} = \Delta T_{i(q)} = \mu\beta_q^{\alpha}\text{sign}\left(e_q\right)\cdot F_q \tag{14}$$

The opening PI gains (k_p and T_i) for the six PI controllers ($PI_{1.1}$ to $PI_{3.2}$) are achieved manually by testing the system in its boundaries, where stated in Table 4. The outputs of LMSRE were taken from [6].

C. ZIEGLER-NICHOLS

A conventional control technique for fine-tuning PI gains named Ziegler–Nichols is presented. This technique initiates by zeroing the K_p and T_i, then increases the K_P until the system critically stable. The K_P at this point named K_{cr} and the critical period named Pcr. The PI gains are determined according to Table 5 [36].

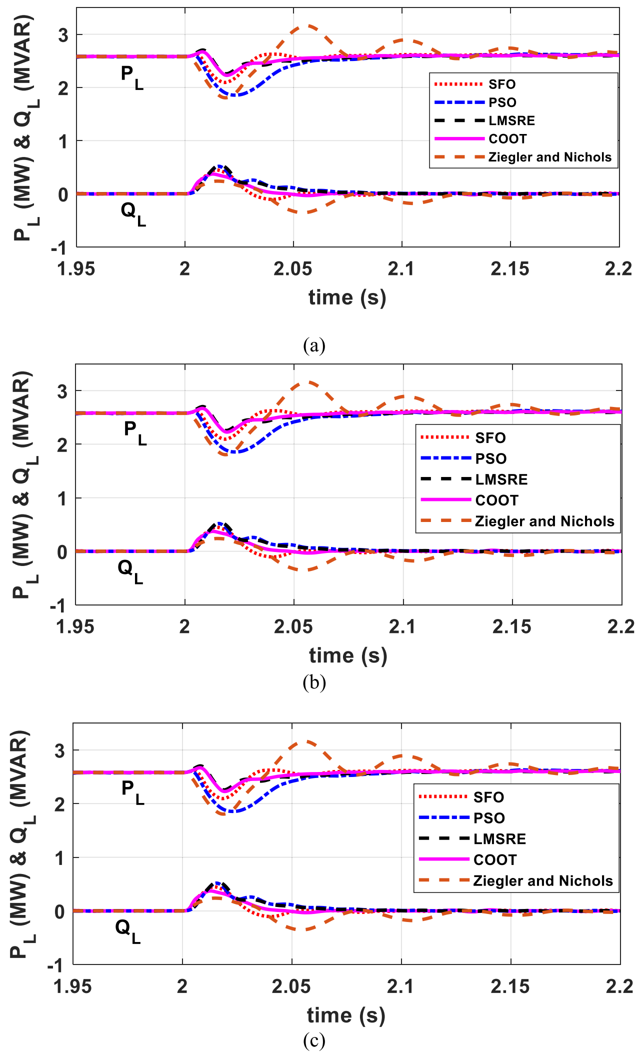

FIGURE 7. The results of CBMO, SFO, PSO, ziegler-nichols and LMSRE for scenario1. (a) Active and reactive load powers in DG 1. (b) Active and reactive load powers in DG 2. (c) Active and reactive load powers in DG 3.

D. OPTIMIZATION USING CBMO

The CMBO mimics the behaviour of a group of American coots swimming in a lake [37]. The primary algorithm was developed based on the behaviours of American coots when travelling in a lake, particularly when confronted with excessive waving and environmental conditions [38], [39]. Lukeman *et al.* examined how to surf scoters change their configurations to travel in line with the big waves. The coots are travelling in a dense flock in front or behind [40]. They organize themselves in two or three dimensions to migrate and change between two phases. The first is an unstructured stage characterized by low density and non-homogeneous coot body directions. However, the other stage is characterized by high density, uniform coot body motions, and velocity. By travelling over a long distance, coots can accelerate their movements in three dimensions.

The coots can move between the first and the second phase utilizing one of two techniques. The first is to accelerate certain nearby coot followers and change their locations so that they are aligned with other coots and enhance the orientations of coot leaders. The second strategy is to promote coot followers with great potential as leaders rather than leaders with poor results. The time necessary to go from

TABLE 7. Results of CBMO, SFO, PSO, ziegler-nichols and LMSRE for scenario1.

Point of compar.	COOT		LMSRE	SFO		PSO		Ziegler-Nichols	
Scenario 1 DG 1									
Optimum size	Y_1	6.21	online	Y_1	6.41	Y_1	2.147	Y_1	3.375
	Y_2	0.0321		Y_2	0.0053	Y_2	0.0057	Y_2	0.004
	Y_3	2.65		Y_3	2.951	Y_3	1.679	Y_3	1.35
	Y_4	1.91		Y_4	0.3471	Y_4	0.339	Y_4	1
MPUS	7.423 %		7.91%	12.91%		20.261%		22.5 %	
MPOS	zero		zero	zero		zero		12.1 %	
T_{set}	0.0382 s		0.0462 s	0.0331 s		0.0541 s		0.165 s	
Ess	0.29 %		0.321%	0.351%		0.405%		1.002 %	
Scenario 1 DG 2									
Optimum size	Y_5	6.15	online	Y_5	5.981	Y_5	1.5691	Y_5	3.15
	Y_6	0.0318		Y_6	0.00409	Y_6	0.0043	Y_6	0.0038
	Y_7	2.59		Y_7	2.5081	Y_7	1.2341	Y_7	1.125
	Y_8	1.95		Y_8	0.2988	Y_8	0.3057	Y_8	0.988
MPUS	7.434 %		7.899%	12.861%		20.11%		22.4 %	
MPOS	zero		zero	zero		zero		11.95 %	
T_{set}	0.03827 s		0.0462 s	0.0327 s		0.0536 s		0.166	
E_{ss}	0.312 %		0.305%	0.361%		0.406%		0.97 %	
Scenario 1 DG 3									
Optimum size	Y_9	6.04	online	Y_9	5.5341	Y_9	1.068	Y_9	2.925
	Y_{10}	0.0307		Y_{10}	0.00312	Y_{10}	0.0032	Y_{10}	0.0036
	Y_{11}	2.51		Y_{11}	2.0991	Y_{11}	0.993	Y_{11}	0.945
	Y_{12}	1.99		Y_{12}	0.24785	Y_{12}	0.2588	Y_{12}	0.961
MPUS	7.451 %		7.572%	12.61%		19.976%		22.31%	
MPOS	zero		zero	zero		zero		11.87 %	
T_{set}	0.03831 s		0.0433 s	0.0323 s		0.0532 s		0.159 s	
E_{ss}	0.289 %		0.311%	0.321%		0.403%		0.95 %	

TABLE 8. The ziegler-nichols critical gains (kcr) and critical periods (Pcr) for the DGs for scenario2.

	Critical gains (k_{cr})	Critical periods (P_{cr})	PI gains	
$PI_{1.1}$	3.33	0.01056	Y_1	1.5
			Y_2	0.0088
$PI_{2.1}$	3.556	0.1896	Y_3	1.6
			Y_4	0.158
$PI_{2.1}$	2.1889	0.01032	Y_5	0.985
			Y_6	0.0086
$PI_{2.2}$	3.444	0.186	Y_7	1.55
			Y_8	0.155
$PI_{3.1}$	2.1556	0.00984	Y_9	0.97
			Y_{10}	0.0082
$PI_{3.2}$	3.3778	0.1812	Y_{11}	1.52
			Y_{12}	0.151

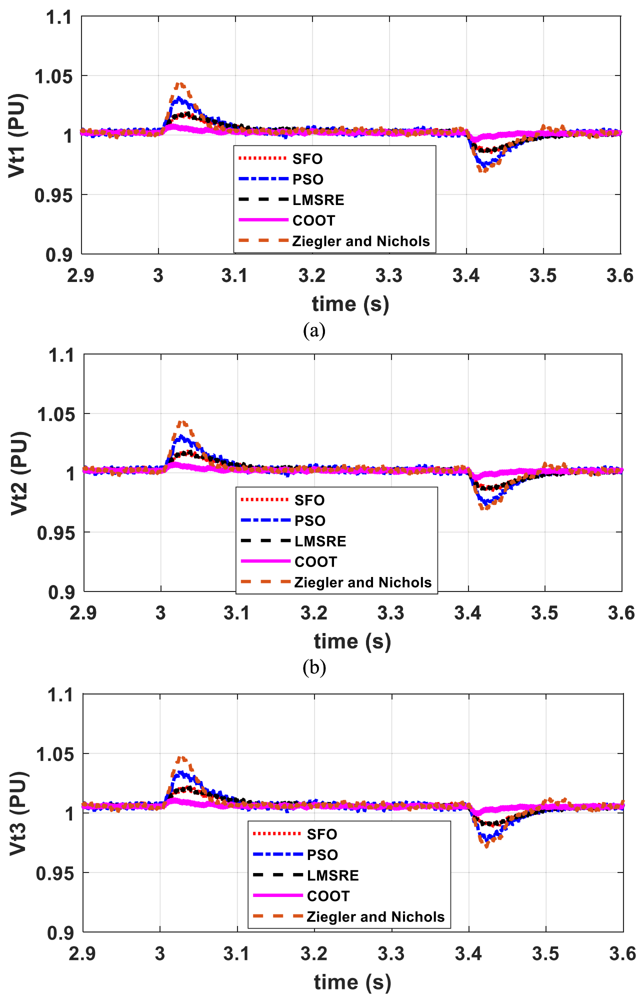

FIGURE 8. The results of CBMO, SFO, PSO, ziegler-nichols and LMSRE for scenario2. (a) Reference voltage of DG 1. (b) Reference voltage of DG 2. (c) Reference voltage of DG 3.

one phase to the next is determined by the density of the coots. The coot leaders are calculated as a percentage of the total estimated coot "populations, Npop," while the rest are coot followers.The places of followers (Poscoots0) and leaders (Posleader) are chosen at random as presented in eq. (15-16), respectively.

$$P_{0Scoots} = Rand_{coot}.\,(U_b - L_b) + L_b \qquad (15)$$

$$P_{0Sleader} = Rand_{leader}.\,(U_b - L_b) + L_b \qquad (16)$$

where U_b denotes the upper limit and L_b denotes the lower limit. All of Coot's followers' fitness Fi_{tcoots} could be calculated utilizing the OF (F_{obj}) as shown in eq. (17).

$$Fit_{coots}(1, i) = F_{obj}(P_{0Scoot}(i)), \quad i = 1 \text{ to } N_{coots} \qquad (17)$$

wher Ncoots is the number of Coot's followers = N_{pop} - $N_{leaders}$ $Gbest_{score}$ and $Gbes_{tpos}$ identify the best global coots

TABLE 9. The results of CBMO, SFO, PSO, ziegler-nichols and LMSRE for scenario2.

Point of compar.	COOT		LMSRE	SFO		PSO		Ziegler-Nichols	
Scenario 2 DG 1									
Optimum size	Y_1	6.374	Online	Y_1	6.4689	Y_1	1.922	Y_1	1.5
	Y_2	0.001		Y_2	0.01248	Y_2	0.0116	Y_2	0.0088
	Y_3	2.54		Y_3	2.2791	Y_3	2.312	Y_3	1.6
	Y_4	0.923		Y_4	0.238	Y_4	0.2313	Y_4	0.158
MPUS	0.49 %		1.89%	2.21%		3.31%		3.5 %	
MPOS	0.986 %		2.22%	2.972%		3.55%		4.4 %	
T_{set}	zero		0.402 s	0.432 s		0.451 s		0.456 s	
E_{ss}	0.38 %		0.43%	0.441%		0.481%		1.091 %	
Scenario 2 DG 2									
Optimum size	Y_5	6.293	Online	Y_5	6.0241	Y_5	1.4023	Y_5	0.985
	Y_6	0.0012		Y_6	0.0093	Y_6	0.0101	Y_6	0.0086
	Y_7	2.511		Y_7	1.861	Y_7	1.7981	Y_7	1.55
	Y_8	0.918		Y_8	0.2072	Y_8	0.1998	Y_8	0.155
MPUS	0.492 %		1.88%	2.121%		3.2751%		3.48 %	
MPOS	0.963 %		2.2%	2.612%		3.642%		4.47 %	
T_{set}	zero		0.403s	0.42892 s		0.4451 s		0.453 s	
E_{ss}	0.392 %		0.52%	0.6651%		0.693%		0.985 %	
Scenario 2 DG 3									
Optimum size	Y_9	6.143	Online	Y_9	5.4971	Y_9	0.8998	Y_9	0.97
	Y_{10}	0.0013		Y_{10}	0.0067	Y_{10}	0.0654	Y_{10}	0.0082
	Y_{11}	2.4895		Y_{11}	1.5782	Y_{11}	1.4876	Y_{11}	1.52
	Y_{12}	0.895		Y_{12}	0.1751	Y_{12}	0.1622	Y_{12}	0.151
MPUS	0.498 %		1.51%	1.746%		2.9091%		3.35 %	
MPOS	0.947 %		2.53%	2.62%		3.72%		4.485 %	
Tset	zero		0.401s	0.4241 s		0.4431 s		0.464 s	
Ess	0.41 %		0.73%	1.033%		1.072%		1.12 %	

TABLE 10. The ziegler-nichols critical gains (kcr) and critical periods (Pcr) for the DGs for scenario 3.

	Critical gains (k_{cr})	Critical periods (P_{cr})	PI gains	
$PI_{1.1}$	3.33	0.0102	Y_1	1.5
			Y_2	0.0085
$PI_{2.1}$	4.44	0.1932	Y_3	2
			Y_4	0.161
$PI_{2.1}$	3.1778	0.00984	Y_5	1.43
			Y_6	0.0082
$PI_{2.2}$	4.3778	0.1824	Y_7	1.97
			Y_8	0.152
$PI_{3.1}$	3.1333	0.00948	Y_9	1.41
			Y_{10}	0.0079
$PI_{3.2}$	4.2667	0.1788	Y_{11}	1.92
			Y_{12}	0.149

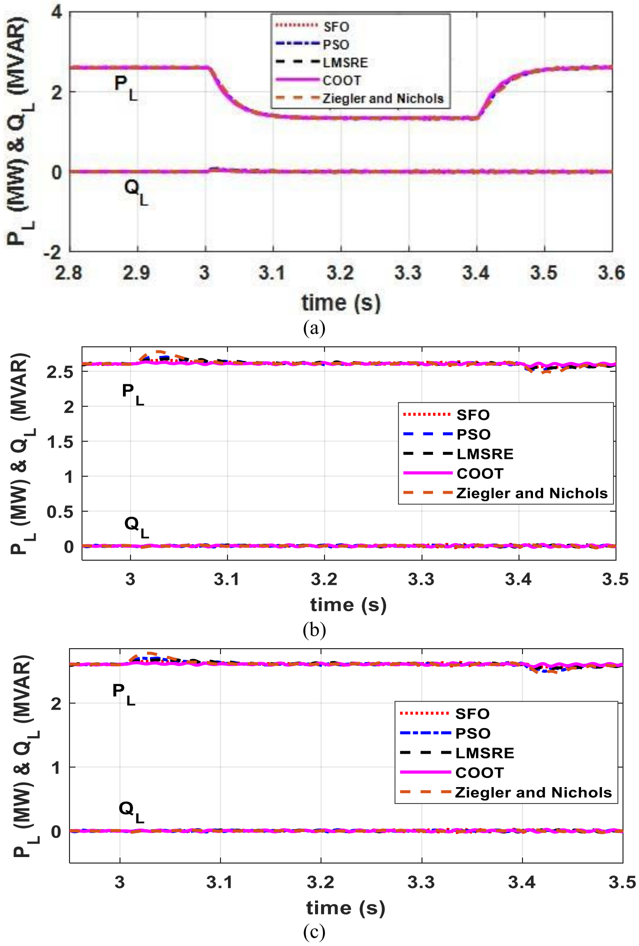

FIGURE 9. **The results of CBMO, SFO, PSO, ziegler-nichols and LMSRE for scenario2. (a) Active and reactive load powers in DG 1. (b) Active and reactive load powers in DG 2. (c) Active and reactive load powers in DG 3.**

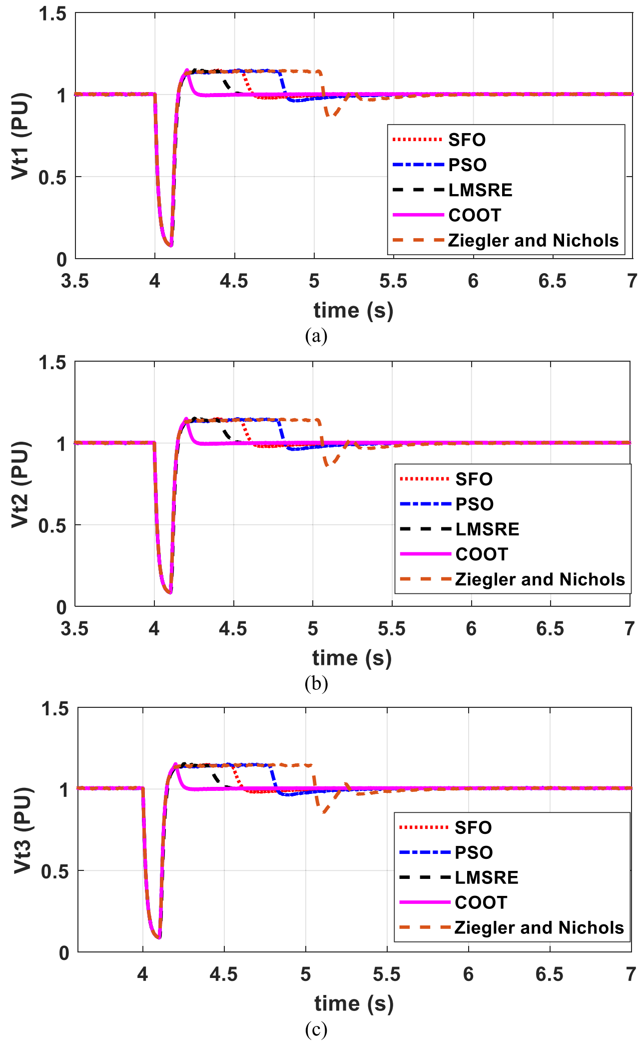

FIGURE 10. **The results of CBMO, SFO, PSO, ziegler-nichols and LMSRE for Scenario3. (a) Reference voltage of DG 1. (b) Reference voltage of DG 2. (c) Reference voltage of DG 3.**

score and its position, respectively as seen in eq. (18).

$$\begin{cases} \text{If } Gbest_{score} > Fit_{coots}(1,i) \text{ then} \\ Gbest_{score} = Fit_{coots}(1,i) \ \& \\ Gbest_{pos} = P_{0Scoot}(i) \end{cases} \tag{18}$$

Furthermore, the OF may be used to assess the fitness of all Coot's leaders by Eq. (19). The $Gbest_{score}$ and its position $Gbest_{pos}$ are distinguished by eq. (20).

$$Fit_{leaders}(1,i) = F_{obj}(P_{leaders}(i)), \quad i \in 1 \text{ to } N_{leaders} \tag{19}$$

$$\begin{cases} \textbf{If } Gbest_{score} > Fit_{leaders}(1,i) \ \textbf{then} \\ Gbest_{score} = Fit_{leaders}(1,i) \ \& \\ Gbest_{pos} = P_{0Sleaders}(i) \end{cases} \tag{20}$$

where $N_{leaders}$ is the number of Coot's leaders ($\%N_{pop}$).

Each of the Coot's followers is allocated to a Coot leader based on a random process, and their locations are updated appropriately, beginning with iteration two and ending with the maximum number of iterations (IT_{max}) as presented in Eqs. (21) and (22). The locations of the new followers are verified to ensure that they are within the parameters specified in Eq. (22).

$$R = 1 + 2.Rand_{coots} \tag{21}$$

$$\begin{aligned} P_{0Scoot}(i) = 2 \cdot Rand_{coots} \cdot \cos(2\pi R) \cdot [P_{0sleaders}(k) \\ - P_{0Scoot}(i)] + P_{0sleaders}(k), \\ \forall \epsilon N_{coots} \text{ and } k \epsilon N_{leaders} \end{aligned} \tag{22}$$

$$\begin{cases} \text{If } P_{0Scoot}(i) > U_b, \text{ then, } P_{0Scoot}(i) = U_b \\ \text{If } P_{0Scoot}(i) < L_b, \text{ then, } P_{0Scoot}(i) = L_b \end{cases} \tag{23}$$

where $Rand_{coots}$ are the randomly produced values of the Coot's followers and $Ran_{dleaders}$ are the randomly created values of the Coot's leaders.

The new fitness of all Coot's followers is assessed and compared to the fitness of the leader. If a follower fitness exceeds that of its associated leader, the follower becomes a leader, and the leader becomes a follower. This process is

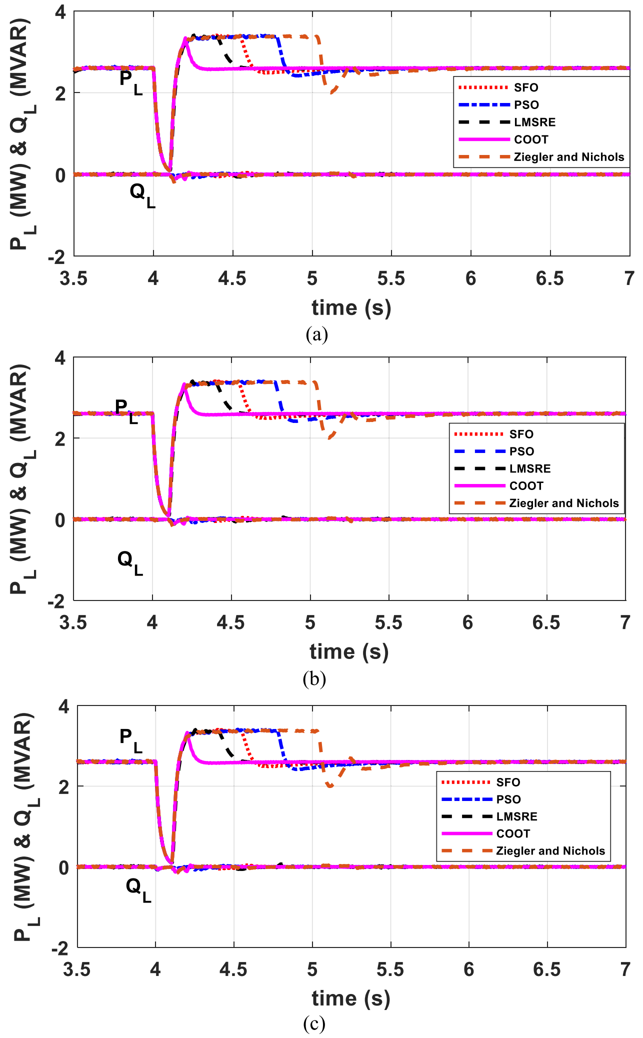

FIGURE 11. The results of CBMO, SFO, PSO, ziegler-nichols and LMSRE for scenario3. (a) Active and reactive load powers in DG 1. (b) Active and reactive load powers in DG 2. (c) Active and reactive load powers in DG 3.

TABLE 11. The results of CBMO, SFO, PSO, ziegler-nichols and LMSRE for scenario3.

Point of compar.	COOT		LMSRE	SFO		PSO		Ziegler-Nichols	
Scenario 3 DG 1									
Optimum size	Y_1	6.5	online	Y_1	6.1341	Y_1	2.1081	Y_1	1.5
	Y_2	0.001		Y_2	0.0042	Y_2	0.00614	Y_2	0.0085
	Y_3	2.6		Y_3	2.4981	Y_3	2.572	Y_3	2
	Y_4	0.9		Y_4	0.1212	Y_4	0.11	Y_4	0.161
MPUS	92.11 %		92.17%	91.639%		93.109%		93.21%	
MPOS	11.55 %		12.41%	11.706%		11.9561%		12.31%	
Tset	0.2447sec		0.491 s	0.56541 s		0.81 s		1.225 s	
E_{ss}	0.31 %		0.251%	0.462%		0.551%		0.97%	
Scenario 3 DG 2									
Optimum size	Y_5	6.365	online	Y_5	6.21	Y_5	2.177	Y_5	1.43
	Y_6	0.0012		Y_6	0.0042	Y_6	0.00598	Y_6	0.0082
	Y_7	2.586		Y_7	2.512	Y_7	2.551	Y_7	1.97
	Y_8	0.946		Y_8	0.1191	Y_8	0.0988	Y_8	0.152
MPUS	91.61 %		91.68%	92.136%		92.141%		92.51%	
MPOS	11.65 %		12.40%	11.75%		11.62%		11.92%	
T_{set}	0.2446 s		0.4917s	0.5721 s		0.8176 s		1.24 s	
Ess	0.324 %		0.337%	0.4952%		0.631%		0.99%	
Scenario 3 DG 3									
Optimum size	Y_9	6.212	online	Y_9	6.12	Y_9	2.21	Y_9	1.41
	Y_{10}	0.0013		Y_{10}	0.0041	Y_{10}	0.0061	Y_{10}	0.0079
	Y_{11}	2.523		Y_{11}	2.472	Y_{11}	2.51	Y_{11}	1.92
	Y_{12}	0.967		Y_{12}	0.121	Y_{12}	0.0106	Y_{12}	0.149
MPUS	91.26 %		91.31%	93.1061%		91.641%		92.62%	
MPOS	12.1 %		12.82%	11.56%		11.53%		12.33%	
T_{set}	0.249 sec		0.4973s	0.57541 s		0.824 s		1.27 s	
E_{ss}	0.434 %		0.671%	0.8421%		1.022%		1.21%	

shown in Eq. (24).

$$\begin{cases} \textbf{If } \mathrm{Fit_{coots}}(1,i) < \mathrm{Fit_{leader}}(1,k) \textbf{ then} \\ \mathrm{Fit_{leader}}(1,k) = \mathrm{Fit_{coots}}(1,i)\ \& \\ \mathrm{P_{0Sleaders}}(k) = \mathrm{P_{0Scoots}}(i) \end{cases} \tag{24}$$

The locations of the leaders are enhanced using a random function, as shown in Eqs. (25), and (26).

$$\begin{cases} \mathrm{B} = 2 - (\mathrm{IT(L)}2/\mathrm{IT_{max}} \\ \mathrm{R} = 1 + 2{\cdot}\mathrm{Rand_{leaders}} \end{cases} \tag{25}$$

$$\big[\mathrm{P_{0sleaders}} = \mathrm{B} \cdot \mathrm{Rand_{leaders}} \cdot \cos(2\pi \mathrm{R}) \cdot \left[\mathrm{Gbest_{pos}} - \mathrm{P_{0sleaders}}(i)\right] + \mathrm{Gbest_{pos}} \tag{26}$$

where IT(L) denotes the iteration L. For the sake of summar, the flowchart of CBMO is presented in Fig. 5.

The best global score and position are determined in eq. (27).

$$\begin{cases} \mathrm{If\ Gbest_{score}} > \mathrm{Fit_{leaders}}(1,i)\ \mathrm{then} \\ \mathrm{Fit_{leader}}(1,k)\ \mathrm{Gbest_{score}}\ \& \\ \mathrm{P_{0Sleaders}}(i) = \mathrm{Gbest_{pos}} \end{cases} \tag{27}$$

VI. SIMULATION RESULTS AND DISCUSSION

This sector is devoted on proving numerical results with the aim of demonstrating the validity and efficacy of the proposed control method based on CMBO. As a major indicator, the effectiveness of the new proposal will be evaluated as its capacity to keep the PCC voltage around the specified ranges in different MG operative modes. The soberness of the controller scheme is demonstrated through the simulation

TABLE 12. PSCAD results for scenario 1.

Exp.	K_{p1}	T_{i1}	K_{p2}	T_{i2}	N_1 $MPUS_1$ (%)	N_3 T_{set1} (%)	N_4 E_{ss1} (%)	N_5 $MPUS_2$ (%)	N_7 T_{set2} (%)	N_8 E_{ss2} (%)	N_9 $MPUS_1$ (%)	N_{11} T_{set1} (%)	N_{12} E_{ss1} (%)
1	0	0	0	0	14.871	0.141	0.7517	15.2631	0.1485	0.62	15.827	0.15988	0.6278
2	-1	1	1	1	26.512	0.1821	1.052	26.82	0.1847	0.7321	27.3	0.22021	1.02
3	1	1	1	1	12.231	0.28445	0.693	12.512	0.2984	0.512	12.92	0.34561	0.538
4	-1	-1	-1	-1	18.732	0.10571	0.283	19.11	0.10024	0.371	19.62	0.08641	1.044
5	1	0	0	0	11.573	0.16788	0.8	11.9162	0.17872	0.5391	12.38	0.19874	0.72086
6	-1	-1	1	1	30.221	0.29312	1.24	30.582	0.3263	0.9551	30.96	0.3761	0.387
7	0	0	0	0	14.872	0.141	0.7517	15.2632	0.1485	0.61	15.827	0.15988	0.6278
8	1	-1	-1	-1	11.412	0.07892	0.377	11.721	0.0796	0.361	12.07	0.0841	0.93
9	1	-1	1	1	14.321	0.26241	0.586	14.621	0.2789	0.4161	15.091	0.30932	0.658
10	0	0	0	1	14.942	0.14889	0.778	15.2881	0.151	0.5942	15.803	0.16811	0.448
11	0	0	0	-1	15.381	0.16251	0.483	15.732	0.15156	0.32	16.29	0.16522	0.9867
12	-1	1	1	-1	27.422	0.18172	0.514	27.721	0.18484	0.792	28.23	0.21531	1.54
13	0	0	0	0	14.871	0.141	0.7517	15.2632	0.1485	0.62	15.827	0.15988	0.6278
14	0	0	0	0	14.872	0.142	0.7517	15.2631	0.1485	0.62	15.827	0.15988	0.6278
15	1	1	-1	-1	9.341	0.0791	0.307	9.682	0.082	0.3652	10.1	0.09288	1.12
16	0	0	0	0	14.871	0.141	0.7517	15.2631	0.1485	0.62	15.827	0.15987	0.6278
17	1	1	-1	1	8.992	0.07672	0.565	9.3142	0.0794	0.38581	9.666	0.08977	0.701
18	-1	-1	-1	1	18.971	0.1061	0.664	19.42	0.1055	0.4752	19.81	0.09181	0.622
19	-1	0	0	0	23.62	0.11292	0.7733	23.962	0.1155	0.3171	24.54	0.12911	0.862
20	1	1	1	-1	12.5062	0.28441	0.185	12.792	0.3038	0.7382	13.2	0.35371	1.469
21	-1	1	-1	1	13.371	0.05141	0.6	13.72	0.0519	0.42	14.1	0.05641	0.725
22	0	0	0	0	14.871	0.142	0.7517	15.2631	0.1485	0.61	15.827	0.15986	0.6278
23	0	-1	0	0	13.681	0.13481	0.8	16.762	0.14	0.5842	17.34	0.14831	0.546
24	-1	-1	1	-1	30.311	0.1651	0.24	30.631	0.1954	0.511	31.08	0.24582	1.159
25	1	-1	-1	1	11.062	0.0792	1.69	11.371	0.9799	1.312	11.71	0.0852	0.73
26	1	-1	1	-1	14.251	0.27891	0.434	14.5361	0.29	0.732	14.96	0.34831	1.47
27	0	1	0	0	14.92	0.14571	0.71	15.251	0.15383	0.45661	15.856	0.17042	0.734
28	0	0	0	0	14.871	0.142	0.7517	15.2631	0.1485	0.62	15.827	0.15986	0.6278
29	-1	1	-1	-1	12.582	0.05961	0.204	12.892	0.0572	0.5262	13.25	0.06222	1.255
30	0	0	1	0	17.21	0.2373	0.719	17.5451	0.24578	0.5261	18.03	0.28211	0.57089
31	0	0	-1	0	10.612	0.07071	0.5522	10.912	0.0731	0.3092	11.305	0.08212	0.8378

outcomes, where taken from the PSCAD/EMTDC environment. To prove the superiority of the CMBO-based methodology developed, it is compared with the results obtained with the LMSRE-based adaptive control, SFO, Ziegler-Nichols and the PSO techniques reported in [6]. The system has been experimented under different microgrid operating modes, 1) isolate the system from the grid (autonomous mode), 2) islanded system exposure to load changes, and 3) islanded system exposure to a 3-phase fault.

A. SCENARIO 1 (OFF-GRID MODE)

In the first scenario, the MG run at normal states and connected to the grid. The MG is abruptly separated from the grid (islanding) at time equal to 2 second. The Ziegler-Nichols Critical gains (k_{cr}) and Critical periods (P_{cr}) for the DGs are reported in Table 6. The optimum PI gains data for the DGs for CBMO, SFO, PSO, Ziegler-Nichols and LMSRE are reported in Table 7. Figs. 6 (a, b, c) depict the reference voltage in the DGs for CBMO, SFO, PSO, Ziegler-Nichols and LMSRE, while Figs. 7 (a, b, c) plot the active and reactive powers for the load in the DGs for CBMO, SFO, PSO, Ziegler-Nichols and LMSRE. It is worthwhile to note that, in Fig. 6a, the MPUS for the stand-alone mode for the offered technique is less than 7.5%. Moreover, the T_{set} based on the 2% criterion for the proposed controller is reduced to 4 ms, and the E_{ss} is 0.29%. Thus, the introduced

TABLE 13. PSCAD results for scenario 2.

Exp.	K_{p1}	T_{i1}	K_{p2}	T_{i2}	N_1 $MPUS_1$(%)	N_2 $MPOS_1$ (%)	N_3 T_{set1} (%)	N_4 E_{ss1} (%)	N_5 $MPUS_1$(%)	N_6 $MPOS_1$ (%)	N_7 T_{set1} (%)	N_8 E_{ss1} (%)	N_9 $MPUS_1$(%)	N_{10} $MPOS_1$ (%)	N_{11} T_{set1} (%)	N_{12} E_{ss1} (%)
1	0	0	0	0	2.9611	3.955	0.4783	0.266	3.221	3.516	0.49578	0.568	3.971	2.7	0.5871	1.48
2	-1	1	1	1	5.32	7.76	0.6458	0.422	5.332	7.197	0.65671	0.673	5.792	6.31	0.7317	1.3
3	1	1	1	1	2.372	4.16	0.4871	0.55	2.522	3.788	0.5068	0.8005	3.132	3.02	0.6177	1.49
4	-1	-1	-1	-1	4.341	5.143	0.4731	0.284	4.521	4.683	0.48211	0.416	5.2341	3.8	0.5098	1.47
5	1	0	0	0	2.2722	3.323	0.4621	0.207	2.5181	2.8879	0.48752	0.639	3.2822	2.119	0.592	1.48
6	-1	-1	1	1	5.651	7.67	0.6207	0.324	5.652	7.16	0.62921	0.105	5.992	6.36	0.6738	0.82
7	0	0	0	0	2.9612	3.955	0.4783	0.266	3.222	3.516	0.49578	0.568	3.971	2.7	0.5872	1.48
8	1	-1	-1	-1	3.1211	3.67	0.4731	0.461	3.361	3.19	0.4821	0.39	4.001	2.4	0.5123	1.311
9	1	-1	1	1	2.442	4.85	0.5068	0.178	2.592	4.5	0.51232	0.572	3.132	3.756	0.6065	1.173
10	0	0	0	1	2.81	4.07	0.4681	0.437	3.0091	3.64	0.4815	0.389	3.631	2.93	0.5065	1.11
11	0	0	0	-1	3.7281	4.37	0.5372	1.445	4.082	3.87	0.5598	1.742	5.1322	2.8	1.001	2.931
12	-1	1	1	-1	6.341	7.11	0.7292	0.98	6.522	6.6	0.792	1.49	7.362	5.56	1.12	0.45
13	0	0	0	0	2.9612	3.955	0.4781	0.266	3.221	3.516	0.49578	0.568	3.972	2.7	0.5871	1.48
14	0	0	0	0	2.9612	3.955	0.4783	0.266	3.221	3.516	0.49578	0.568	3.971	2.7	0.5873	1.48
15	1	1	-1	-1	3.151	3.88	0.4818	0.364	3.421	3.45	0.49312	0.634	4.261	2.57	0.5433	1.75
16	0	0	0	0	2.9612	3.955	0.4783	0.266	3.222	3.516	0.49578	0.568	3.971	2.7	0.5873	1.48
17	1	1	-1	1	2.741	3.92	0.4789	0.5	2.862	3.616	0.49272	0.173	3.371	2.916	0.5181	0.963
18	-1	-1	-1	1	4.232	5.29	0.4731	0.568	4.262	4.93	0.47387	0.28	4.672	4.25	0.4848	0.836
19	-1	0	0	0	4.521	6.595	0.5318	0.219	4.72	6.18	0.54282	0.838	5.362	5.324	0.5962	1.68
20	1	1	1	-1	3.872	4.73	0.7292	1.404	4.151	4.31	0.82681	1.912	5.091	3.31	1.311	2.16
21	-1	1	-1	1	3.781	5.25	0.4791	0.483	3.842	4.896	0.492	0.221	4.32	4.16	0.5122	0.98
22	0	0	0	0	2.962	3.955	0.4781	0.266	3.221	3.516	0.49578	0.568	3.971	2.7	0.5871	1.48
23	0	-1	0	0	3.051	4.1	0.4737	0.311	3.2892	3.66	0.492	0.52	4.002	2.895	0.5651	1.45
24	-1	-1	1	-1	6.242	6.85	0.6625	1.11	6.41	6.35	0.69572	1.57	7.11	5.359	1.21	1.75
25	1	-1	-1	1	3.142	4.82	0.4792	0.456	3.352	4.32	0.48732	0.2	3.772	3.62	0.5128	0.775
26	1	-1	1	-1	3.461	4.51	0.7151	1.41	3.722	4.1	0.91791	1.92	4.642	3.17	1.4212	3.56
27	0	1	0	0	2.922	3.84	0.4763	0.265	3.171	3.379	0.49851	0.794	3.981	2.536	0.5653	1.72
28	0	0	0	0	2.961	3.955	0.4783	0.266	3.222	3.516	0.49578	0.568	3.972	2.7	0.5871	1.48
29	-1	1	-1	-1	4.482	5.134	0.4792	0.3	4.71	4.64	0.49041	0.69	5.462	3.7	0.5232	1.77
30	0	0	1	0	3.651	6.09	0.5458	0.6358	3.822	5.72	0.56232	0.953	4.472	4.87	0.7898	1.77
31	0	0	-1	0	3.521	4.487	0.4822	0.541	3.631	4.09	0.49021	0.191	4.161	3.348	0.5178	0.9955

optimizer offers the least overshoots, quick damping, and applicable E_{ss}. It is worthy to note that the CBMO is much better in MPUS, MPOS, T_{set}, and Ess over LMSRE-based adaptive control, SFO, Ziegler-Nichols and the PSO techniques, which verify the rigidity, validation, and applicability of the presented CBMO over LMSRE-based adaptive control, SFO, Ziegler-Nichols and the PSO techniques.

B. SCENARIO 2 (LOAD CHANGING)

In the second scenario, the MG run at normal states and in the stand-alone mode. The MG initially operates implemented with RLC loads, where stated in Table 1. R12 is varied from 150 Ω to 300 Ω at t = 3 s and back to its original state at time = 3.4 s. The Ziegler-Nichols Critical gains (k_{cr}) and Critical periods (P_{cr}) for the DGs are reported in Table 8. The optimum PI gains data for the DGs for CBMO, SFO, PSO, Ziegler-Nichols and LMSRE are introduced in Table 9. Figs. 8 (a, b, c) shows the reference voltage in each DG for CBMO, LMSRE, SFO, Ziegler-Nichols and PSO. Figs. 9 (a, b, c) plot the active and reactive powers for the load in the DGs for CBMO, SFO, PSO, Ziegler-Nichols and LMSRE. It is worthy to note that, in Fig. 8a, the MPUS and MPOS for the load variability scenario for the offered technique are below 1%. Furthermore, the T_{set} relies on the 2% criterion for the proposed controller is reduced to zero seconds, and the E_{ss} is 0.38%. Thus, the introduced optimizer offers the least overshoots, quick damping, and applicable E_{ss}. It is worthy to recognize that, in Fig. 8a, the real load power of DG 1 is reduced from 2.6 MW to 0.5 MW and restored to its original value efficiently at t=3.4 s. Alternatively, the real load powers for the rest DGs have quick damping with lesser oscillations. It is worthy to note that the CBMO is much better in MPUS, MPOS, T_{set}, and E_{ss} over LMSRE-based adaptive control, SFO,

TABLE 14. PSCAD results for scenario 3.

Exp.	K_{p1}	T_{i1}	K_{p2}	T_{i2}	N_1 $MPUS_1$(%)	N_2 $MPOS_1$ (%)	N_3 T_{set1} (%)	N_4 E_{ss1} (%)	N_5 $MPUS_1$(%)	N_6 $MPOS_1$ (%)	N_7 T_{set1} (%)	N_8 E_{ss1} (%)	N_9 $MPUS_1$(%)	N_{10} $MPOS_1$ (%)	N_{11} T_{set1} (%)	N_{12} E_{ss1} (%)
1	0	0	0	0	92.391	6.58	1.8858	0.3356	90.1121	6.244	1.6892	0.477	87.8061	5.52	1.1668	0.771
2	-1	1	1	1	92.292	7.42	3.001	0.328	90.001	7.12	2.6971	10020 00	87.631	6.55	2.1167	0.585
3	1	1	1	1	92.311	7.53	2.7861	0.4	90.002	7.2	2.681	0.9	87.662	6.634	2.1861	0.55
4	-1	-1	-1	-1	92.541	7.37	5.1351	1.7659	90.311	7.14	5.00341	1.498	88.0492	6.833	5.677	0.987
5	1	0	0	0	92.388	6.738	1.8363	0.4929	90.102	6.39	1.6862	0.351	87.792	5.68	1.161	0.807
6	-1	-1	1	1	92.293	7.28	6.9871	1.987	89.988	6.97	6.1541	0.799	87.6541	6.37	5.9986	1.45
7	0	0	0	0	92.391	6.58	1.8858	0.3356	90.111	6.244	1.6892	0.477	87.8062	5.52	1.1668	0.771
8	1	-1	-1	-1	92.443	7.89	4.31	0.95	90.181	7.7177	4.1341	1.09	87.882	7.38	4.51	0.899
9	1	-1	1	1	92.301	7.46	5.22	7.63	89.991	7.144	4.7651	6.99	87.642	6.53	4.5231	5.498
10	0	0	0	1	92.343	7.6	2.31	0.277	90.034	7.28	2.2221	0.288	87.712	6.659	2.0161	0.334
11	0	0	0	-1	92.676	3.76	0.5532	0.4198	90.51	3.349	0.52861	0.3333	88.2541	2.3	0.4781	0.192
12	-1	1	1	-1	92.581	4.77	0.6891	0.53	90.37	4.4	0.6172	1.2	88.11	3.5	0.5284	923.4
13	0	0	0	0	92.392	6.58	1.8858	0.3356	90.1121	6.244	1.6892	0.477	87.8062	5.52	1.1668	0.771
14	0	0	0	0	92.392	6.58	1.8858	0.3356	90.1121	6.244	1.6892	0.477	87.8062	5.52	1.1668	0.771
15	1	1	-1	-1	92.541	7.8	3.2021	0.274	90.321	7.61	3.20271	0.457	88.041	7.19	3.2027	0.355
16	0	0	0	0	92.391	6.58	1.8858	0.3356	90.1121	6.244	1.6892	0.477	87.8062	5.52	1.1668	0.771
17	1	1	-1	1	92.32	8.17	6.22	4.56	89.994	7.91	6.0781	8.76	87.6651	7.49	5.9871	6.76
18	-1	-1	-1	1	92.291	8.07	7.1361	1.87	89.974	7.8	7.0571	1.43	87.6431	7.339	7.451	0.993
19	-1	0	0	0	92.381	6.9	2.1081	0.559	90.074	6.57	2.0412	0.506	87.7581	5.9	1.3193	0.44
20	1	1	1	-1	92.571	4.6	0.6222	0.51	90.351	4.21	0.57482	0.35	88.0851	3.29	0.4866	0.375
21	-1	1	-1	1	92.32	7.88	7.1761	8.033	89.981	7.61	6.8542	7.995	87.642	7.239	6.3608	8.12
22	0	0	0	0	92.391	6.58	1.8858	0.3356	90.1121	6.244	1.6892	0.477	87.8062	5.52	1.1668	0.771
23	0	-1	0	0	92.412	6.59	2.3361	0.249	90.132	6.25	2.2111	0.371	87.8021	5.539	1.6638	0.332
24	-1	-1	1	-1	92.552	4.77	0.8888	0.51	90.332	4.41	0.81382	0.46	88.031	3.5	0.6031	0.68
25	1	-1	-1	1	92.292	8.42	6.671	1.78	89.981	8.13	6.482	0.9876	87.662	7.69	6.7061	2.56
26	1	-1	1	-1	92.581	4.94	0.7418	0.75	90.372	4.54	0.69191	0.87	88.0812	3.61	0.5291	1.2
27	0	1	0	0	92.427	6.7	1.5362	0.345	90.1491	6.36	1.4612	0.285	87.8231	5.65	0.9862	0.471
28	0	0	0	0	92.391	6.58	1.8858	0.3356	90.1122	6.244	1.6892	0.477	87.8062	5.52	1.1668	0.771
29	-1	1	-1	-1	92.552	7.7	6.872	5.6	90.331	7.539	6.5671	5.1	88.051	7.08	6.1261	6.1
30	0	0	1	0	92.382	7.19	2.3611	4.52	90.0742	6.86	2.2131	0.347	87.7421	6.18	1.6381	0.525
31	0	0	-1	0	92.3451	8.03	5.002	7.44	90.0471	7.763	4.91	5.5	87.7271	7.278	4.61	3.25

Ziegler-Nichols and the PSO techniques, which verify the rigidity, validation, and applicability of the presented CBMO over LMSRE-based adaptive control, SFO, Ziegler-Nichols and the PSO techniques.

C. SCENARIO 3 (3-PHASE FAULT)

In scenario 3, the MG run at normal states and in the stand-alone mode. Then, a 3-phase fault is applied at PCC 1 at t=4 s, and the fault is removed at t=4.1 s. The Ziegler-Nichols Critical gains (k_{cr}) and Critical periods (P_{cr}) for the DGs are reported in Table 10. Table 11 introduces the optimum PI gains data in the DGs for CBMO, SFO, PSO, Ziegler-Nichols and LMSRE. Figs. 10 (a, b, c) plot the reference voltage in the DGs for CBMO, LMSRE, SFO, Ziegler-Nichols and PSO. Figs. 11 (a, b, c) show the active and reactive powers for the load in each DG for CBMO, SFO, PSO, Ziegler-Nichols and LMSRE. It is worthy to note that, in Fig. 10a, the T_{set} relies on the 2% criterion for the offered optimizer is 24 ms, and the E_{ss} is 0.31%. Thus, the introduced opimizer offers quick damping and applicable E_{ss}. which verify the rigidity, validation, and applicability of the presented CBMO over LMSRE-based adaptive control, SFO, Ziegler-Nichols and the PSO techniques.

VII. CONCLUSION

A new PI controller optimal design based on CMBO has been developed in this paper. The new proposal considers various PI controller parameters to enhance microgrid efficiency. The control method employs six PI controllers.

Extensive simulations were performed on a benchmark MG, with the aim of validating the developed methodology. The practicality of the control scheme is demonstrated by the simulation data, which is taken from the PSCAD/EMTDC software. The results evidenced that the proposed controller

TABLE 15. RSM model constants for scenario 1.

Cons.	scenario (1)								
	N_1	N_3	N_4	N_5	N_7	N_8	N_9	N_{11}	N_{12}
M_1	14.7832	0.14125	0.74541	-0.0094	0.14012	0.5251	15.8961	0.16001	0.62901
M_2	-5.3351	0.01859	0.00371	-5.351	0.06942	0.0155	-5.3771	0.02356	-0.01542
M_3	-1.3951	-0.00882	-0.08242	-1.559	-0.06111	-0.0448	-1.5572	-0.00936	0.08642
M_4	3.8842	0.08121	0.02342	3.869	0.03881	0.0781	3.8971	0.10921	0.04711
M_5	-0.0731	0.00490	0.26891	-0.067	0.05622	0.0605	-0.0802	0.00491	-0.28581
M_6	2.9052	-0.0023	0.0492	2.521	0.01681	-0.010	2.4841	0.0038	0.16112
M_7	-0.3911	-0.0025	0.0171	0.588	0.01661	0.083	0.6222	-0.0008	0.00961
M_8	-0.7762	0.0112	-0.1022	-1.190	0.02912	-0.020	-1.3081	0.0220	0.07401
M_9	0.4792	0.0130	-0.1072	0.092	0.02102	0.009	0.0712	0.0065	0.08702
M_{10}	0.6482	0.01378	-0.08002	0.665	-0.03852	-0.0597	0.6652	0.01883	-0.08052
M_{11}	-2.3941	0.01857	-0.14601	-2.392	-0.03911	-0.0777	-2.3851	0.01529	0.01212
M_{12}	-0.0591	-0.00870	-0.00521	-0.066	0.04692	0.0039	-0.0581	-0.01149	-0.00741
M_{13}	0.3411	0.00225	0.08012	0.341	0.05471	0.0623	0.3532	-0.00617	0.02611
M_{14}	-0.0391	-0.00765	-0.07162	-0.046	-0.06492	-0.0986	-0.0402	-0.00686	-0.01211
M_{15}	-0.0962	0.00763	-0.00941	-0.098	-0.04901	-0.0690	-0.0901	0.00566	-0.09152

TABLE 16. RSM model constants for scenario 2.

Cons.	scenario (2)											
	N_1	N_2	N_3	N_4	N_5	N_6	N_7	N_8	N_9	N_{10}	N_{11}	N_{12}
M_1	3.00021	4.118	0.477791	0.3454	3.25181	3.683	0.49321	0.6417	4.00412	2.866	0.59591	1.572
M_2	-1.01772	-1.0522	-0.015622	0.0467	-0.96842	-1.0263	-0.0024	0.0532	-0.9217	-0.9968	0.01671	0.2003
M_3	-0.04001	-0.0622	0.006102	0.0092	-0.03492	-0.0565	0.00422	0.0786	0.01142	-0.0849	-0.00361	-0.0312
M_4	0.37892	0.6742	0.074551	0.1698	0.37561	0.6617	0.09531	0.3778	0.41531	0.6084	0.21201	0.2013
M_5	-0.34881	0.1329	-0.03558	-0.2133	-0.41452	0.1586	-0.0558	-0.4084	-0.5832	0.2585	-0.16421	-0.4281
M_6	0.3502	0.650	0.01972	-0.2250	0.3201	0.655	0.02501	0.011	0.27721	0.662	-0.01302	-0.099
M_7	-0.0612	-0.339	-0.00231	-0.1500	-0.0591	-0.359	0.00411	-0.071	-0.05382	-0.344	-0.04071	-0.094
M_8	0.5392	0.980	0.03662	0.1504	0.4361	1.026	0.03612	-0.156	0.27121	1.050	0.04782	-0.296
M_9	0.2181	-0.089	0.02522	0.5030	0.2562	-0.124	0.03051	0.338	0.33721	-0.194	0.14731	0.341
M_{10}	0.03312	-0.0913	-0.006272	0.0259	0.02312	-0.0723	-0.0142	-0.0166	0.02461	-0.0682	-0.00391	-0.005
M_{11}	-0.41941	-0.4133	-0.014261	0.0350	-0.41191	-0.3773	-0.0015	0.0985	-0.37412	-0.3706	0.01211	0.270
M_{12}	-0.02942	-0.0483	-0.020161	-0.0674	-0.01692	-0.0460	-0.0322	-0.0140	-0.01161	-0.0499	-0.03752	-0.180
M_{13}	0.04811	0.0387	0.004061	0.0285	0.05191	0.0191	-0.0011	0.0173	0.04962	0.0174	-0.01372	-0.186
M_{14}	-0.12192	-0.1388	-0.005262	0.0404	-0.13062	-0.1306	0.00131	0.0175	-0.13542	-0.1244	0.01682	0.193
M_{15}	-0.18441	-0.0133	-0.036151	-0.2518	-0.18811	-0.0321	-0.0575	-0.2178	-0.20661	-0.0268	-0.14621	-0.024

TABLE 17. RSM model constants for scenario 3.

Cons.	scenario (3)											
	N_1	N_2	N_3	N_4	N_5	N_6	N_7	N_8	N_9	N_{10}	N_{11}	N_{12}
M_1	92.4011	6.582	1.776	0.8221	90.1205	6.238	1.631	0.493	87.8113	5.507	1.103	-6.81
M_2	-0.00283	0.0771	-0.469	-0.214	-0.00338	0.073	-0.418	0.088	-0.00295	0.067	-0.384	-51.31
M_3	-0.00273	-0.0121	-0.4062	0.1721	0.012891	-0.0081	-0.3652	0.5981	0.01412	-0.008	-0.538	51.82
M_4	0.01450	-0.8541	-1.578	-0.838	0.01912	-0.9091	-1.6152	-1.151	0.01488	-1.076	-1.779	50.21
M_5	0.00954	0.9021	1.3592	0.8641	-0.17268	0.9032	1.2701	0.946	-0.20371	0.9902	1.1781	-50.42
M_6	-0.0293	0.2361	0.3272	-0.865	-0.0424	0.2462	0.3021	-0.082	-0.0434	0.2991	0.2132	16.32
M_7	0.0146	0.0621	0.2912	-1.094	0.0093	0.072	0.275	-0.182	-0.0049	0.1041	0.2981	16.01
M_8	-0.0513	1.0272	2.0351	4.592	-0.06981	1.0782	1.9951	2.415	-0.08281	1.2382	2.0931	17.52
M_9	-0.12807	-0.9031	-0.2192	-1.043	0.1373	-0.9191	-0.1862	-0.198	0.16471	-1.012	0.2212	15.91
M_{10}	0.00363	-0.0561	-0.1061	-0.859	0.004811	-0.0592	-0.0781	-0.613	0.00907	-0.059	0.014	-58.51
M_{11}	-0.0292	-0.0612	0.2334	0.9771	0.00957	-0.0688	0.2512	0.6981	0.01182	-0.071	0.2312	-57.12
M_{12}	0.00725	0.0191	0.0801	0.5052	0.008312	0.0182	0.1022	0.7931	0.01257	0.0181	0.1062	58.31
M_{13}	0.0053	0.00412	-0.4332	-1.328	-0.00919	-0.0011	-0.3682	-1.486	-0.00582	0.0131	-0.231	56.32
M_{14}	-0.00651	-0.0083	-0.4473	-0.182	-0.00795	-0.0102	-0.4042	0.2792	-0.01483	0.0152	-0.443	-57.61
M_{15}	-0.0512	0.5521	0.462	0.0241	-0.01395	0.5893	0.3772	-0.315	-0.01883	0.684	0.357	-58.1

is able to keep stable the active and reactive powers simultaneously and effectively regulate the voltage profile. Results obtained also confirmed rapid damping in transient response with a quick T_{set} and a slight E_{ss} under several microgrid operating conditions, 1) isolating the system from the grid (autonomous mode), 2) islanded system exposure to load change, and 3) islanded system exposure to a 3 phase fault.

The suggested optimizer was validated by comparing its results with those achieved using the LMSRE-based adaptive control, SFO, Ziegler-Nichols, and the PSO techniques. In all the studied scenarios, CBMO attained lower values of the transient responses than those obtained via the LMSRE-based adaptive control, SFO, Ziegler-Nichols and the PSO techniques. More precisely, the CMBO was able to improve the voltage MPUS up to 74%, 77.8%, 85% and 86% compared with LMSRE-based adaptive control, SFO, Ziegler-Nichols and the PSO techniques, respectively. The new proposal was also able to reduce T_{set} by 100% in scenario 2, when the MG suffers an abrupt load variation in off-grid mode.

The upcoming research will concentration on strengthening the presented CBMO based PI controller to modify the power system requests, energy storage strategies, and smart-grids, reaching optimal comebacks in the green energy systems.

APPENDIX

See Tables 12–17.

ACKNOWLEDGMENT

This work was supported by the Researchers Supporting Project number (RSP-2021/258), King Saud University, Riyadh, Saudi Arabia.

REFERENCES

[1] A. S. Menesy, H. M. Sultan, S. Kamel, R. A. Turky, A. Al-Durra, and H. M. Hasanien, "Optimal values of unknown parameters of polymer electrolyte membrane fuel cells using improved chaotic electromagnetic field optimization," in *Proc. IEEE Ind. Appl. Soc. Annu. Meeting*, Oct. 2020, pp. 1–8.

[2] M. A. Soliman, H. M. Hasanien, A. Al-Durra, and M. Debouza, "High performance frequency converter controlled variable-speed wind generator using linear-quadratic regulator controller," *IEEE Trans. Ind. Appl.*, vol. 56, no. 5, pp. 5489–5498, Sep. 2020.

[3] I. Alsaidan, M. A. M. Shaheen, H. M. Hasanien, M. Alaraj, and A. S. Alnafisah, "Proton exchange membrane fuel cells modeling using chaos game optimization technique," *Sustainability*, vol. 13, no. 14, p. 7911, Jul. 2021.

[4] M. A. M. Shaheen, H. M. Hasanien, M. S. E. Moursi, and A. A. El-Fergany, "Precise modeling of PEM fuel cell using improved chaotic MayFly optimization algorithm," *Int. J. Energy Res.*, vol. 45, no. 13, pp. 18754–18769, Oct. 2021.

[5] M. A. Soliman, H. M. Hasanien, H. Z. Azazi, E. E. El-Kholy, and S. A. Mahmoud, "An adaptive fuzzy logic control strategy for performance enhancement of a grid-connected PMSG-based wind turbine," *IEEE Trans. Ind. Informat.*, vol. 15, no. 6, pp. 3163–3173, Jun. 2019.

[6] A. M. Hussien, R. A. Turky, H. M. Hasanien, and A. Al-Durra, "LMSRE-based adaptive PI controller for enhancing the performance of an autonomous operation of microgrids," *IEEE Access*, vol. 9, pp. 90577–90586, 2021.

[7] D. Kumar, H. D. Mathur, S. Bhanot, and R. C. Bansal, "Forecasting of solar and wind power using LSTM RNN for load frequency control in isolated microgrid," *Int. J. Model. Simul.*, vol. 41, no. 4, pp. 311–323, Jul. 2021.

[8] T. Adefarati, R. C. Bansal, M. Bettayeb, and R. Naidoo, "Optimal energy management of a PV-WTG-BSS-DG microgrid system," *Energy*, vol. 217, Feb. 2021, Art. no. 119538.

[9] S. Areekkara, R. Kumar, and R. C. Bansal, "An intelligent multi agent based approach for autonomous energy management in a microgrid," *Electr. Power Compon. Syst.*, vol. 49, nos. 1–2, pp. 18–31, Jan. 2021.

[10] A. M. Taher, H. M. Hasanien, A. R. Ginidi, and A. T. M. Taha, "Hierarchical model predictive control for performance enhancement of autonomous microgrids," *Ain Shams Eng. J.*, vol. 12, no. 2, pp. 1867–1881, Jun. 2021.

[11] A. Kumar and T. Ghose, "A Newton–Raphson-based unified load flow of grid-connected and islanded AC-DC microgrids," *Int. Trans. Elect. Energy Syst.*, vol. 31, no. 11, 2021, Art. no. e13075.

[12] C. Raj, D. N. Gaonkar, and J. M. Guerrero, "Improved *P-f/Q-V* and *P-V/Q-f* droop controllers for parallel distributed generation inverters in AC microgrid," *Sustain. Cities Soc.*, vol. 41, pp. 421–442, Aug. 2018.
[13] R. An, Z. Liu, J. Liu, and B. Liu, "A comprehensive solution to decentralized coordinative control of distributed generations in islanded microgrid based on dual-frequency-droop," *IEEE Trans. Power Electron.*, vol. 37, no. 3, pp. 3583–3598, Mar. 2022.
[14] Z. Ozkan and A. M. Hava, "Inductor saturation compensation in three-phase three-wire voltage-source converters via inverse system dynamics," *IEEE Trans. Ind. Electron.*, vol. 69, no. 5, pp. 4309–4319, May 2022.
[15] S. D'Arco, J. A. Suul, and O. B. Fosso, "Automatic tuning of cascaded controllers for power converters using eigenvalue parametric sensitivities," *IEEE Trans. Ind. Appl.*, vol. 51, no. 2, pp. 1743–1753, Mar./Apr. 2015.
[16] M. Saleh, Y. Esa, and A. Mohamed, "Centralized control for DC microgrid using finite state machine," in *Proc. IEEE Power Energy Soc. Innov. Smart Grid Technol. Conf. (ISGT)*, Apr. 2017, pp. 1–5.
[17] W. S. W. Wang, D. E. Davison, and E. J. Davison, "Controller design for multivariable linear time-invariant unknown systems," *IEEE Trans. Autom. Control* vol. 58, no. 9, pp. 2292–2306, Sep. 2013.
[18] Y. K. Bhateshvar and H. D. Mathur, "Power–frequency balance with superconducting magnetic energy storage using optimized intelligent controller," *Energetika*, vol. 60, no. 3, pp. 149–161, Nov. 2014.
[19] A. M. Hussien, H. M. Hasanien, and S. F. Mekhamer, "Sunflower optimization algorithm-based optimal PI control for enhancing the performance of an autonomous operation of a microgrid," *Ain Shams Eng. J.*, vol. 12, no. 2, pp. 1883–1893, Jun. 2021.
[20] S. Patel, B. Mohanty, and H. M. Hasanien, "Competition over resources optimized fuzzy TIDF controller for frequency stabilization of hybrid micro-grid system," *Int. Trans. Electr. Energy Syst.*, vol. 30, no. 9, 2020, Art. no. e12513.
[21] M. N. Ambia, H. M. Hasanien, A. Al-Durra, and S. M. Muyeen, "Harmony search algorithm-based controller parameters optimization for a distributed-generation system," *IEEE Trans. Power Del.*, vol. 30, no. 1, pp. 246–255, Feb. 2015.
[22] A. M. Hussien, S. F. Mekhamer, and H. M. Hasanien, "Cuttlefish optimization algorithm based optimal PI controller for performance enhancement of an autonomous operation of a DG system," in *Proc. 2nd Int. Conf. Smart Power Internet Energy Syst. (SPIES)*, Sep. 2020, pp. 293–298.
[23] M. A. M. Shaheen, H. M. Hasanien, and A. Al-Durra, "Solving of optimal power flow problem including renewable energy resources using HEAP optimization algorithm," *IEEE Access*, vol. 9, pp. 35846–35863, 2021.
[24] N. M. Hassan, R. A. Swief, M. Z. Kamh, H. M. Hasanien, and A. Y. Abdelaziz, "Toward centralized/decentralized controlled power flow applying whale versus genetic optimization algorithms," *Int. J. Recent Tech. Eng.*, vol. 8, no. 4, pp. 1–8, Nov. 2019.
[25] M. A. M. Shaheen, H. M. Hasanien, S. F. Mekhamer, and H. E. A. Talaat, "Optimal power flow of power systems including distributed generation units using sunflower optimization algorithm," *IEEE Access*, vol. 7, pp. 109289–109300, 2019.
[26] M. A. M. Shaheen, S. F. Mekhamer, H. M. Hasanien, and H. E. A. Talaat, "Optimal power flow of power systems using hybrid firefly and particle swarm optimization technique," in *Proc. 21st Int. Middle East Power Syst. Conf. (MEPCON)*, Dec. 2019, pp. 232–237.
[27] M. Qais, H. M. Hasanien, and S. Alghuwainem, "Salp swarm algorithm-based TS-FLCs for MPPT and fault ride-through capability enhancement of wind generators," *ISA Trans.*, vol. 101, pp. 211–224, Jun. 2020.
[28] M. A. M. Shaheen, D. Yousri, A. Fathy, H. M. Hasanien, A. Alkuhayli, and S. M. Muyeen, "A novel application of improved marine predators algorithm and particle swarm optimization for solving the ORPD problem," *Energies*, vol. 13, no. 21, p. 5679, Oct. 2020.
[29] H. Y. Mahmoud, H. M. Hasanien, A. H. Besheer, and A. Y. Abdelaziz, "Hybrid cuckoo search algorithm and grey wolf optimiser-based optimal control strategy for performance enhancement of HVDC-based offshore wind farms," *IET Gener., Transmiss. Distrib.*, vol. 14, no. 10, pp. 1902–1911, May 2020.
[30] A. H. A. Elmomen, H. M. Hasanien, and A. Y. Abdelaziz, "Development of optimal PI controllers of an inverter–based decentralized energy generation system based on equilibrium optimization algorithm," *Int. J. Renew. Energy Res.*, vol. 11, no. 3, pp. 1095–1106, 2021.
[31] R. A. Swief, N. M. Hassan, H. M. Hasanien, A. Y. Abdelaziz, and M. Z. Kamh, "AC&DC optimal power flow incorporating centralized/decentralized multi-region grid control employing the whale algorithm," *Ain Shams Eng. J.*, vol. 12, no. 2, pp. 1907–1922, Jun. 2021.
[32] A. E. Chaib, H. R. E. H. Bouchekara, R. Mehasni, and M. A. Abido, "Optimal power flow with emission and non-smooth cost functions using backtracking search optimization algorithm," *Int. J. Electr. Power Energy Syst.*, vol. 81, pp. 64–77, Oct. 2016.
[33] H. M. Hasanien, A. S. Abd-Rabou, and S. M. Sakr, "Design optimization of transverse flux linear motor for weight reduction and performance improvement using response surface methodology and genetic algorithms," *IEEE Trans. Energy Convers.*, vol. 25, no. 3, pp. 598–605, Sep. 2010.
[34] I. Y. Kim and O. L. de Weck, "Adaptive weighted sum method for multi-objective optimization: A new method for Pareto front generation," *Struct. Multidisciplinary Optim.*, vol. 31, no. 2, pp. 105–116, Feb. 2006.
[35] M. H. Qais, H. M. Hasanien, and S. Alghuwainem, "A novel LMSRE-based adaptive PI control scheme for grid-integrated PMSG-based variable-speed wind turbine," *Int. J. Electr. Power Energy Syst.*, vol. 125, Feb. 2021, Art. no. 106505.
[36] O. Katsuhiko, *Modern Control Engineering*. Upper Saddle River, NJ, USA: Prentice-Hall, 2010.
[37] I. Naruei and F. Keynia, "A new optimization method based on COOT bird natural life model," *Expert Syst. Appl.*, vol. 183, Nov. 2021, Art. no. 115352.
[38] D. McNair and C. Cramer-Burke, "Breeding ecology of American and Caribbean coots at Southgate Pond, St. Croix: Use of woody vegetation," *Wilson J. Ornithol.*, vol. 118, no. 2, pp. 208–217, 2006, doi: 10.1676/05-020.1.
[39] D. Shizuka and B. E. Lyon, "Coots use hatch order to learn to recognize and reject conspecific brood parasitic chicks," *Nature*, vol. 463, no. 7278, pp. 223–226, Jan. 2010, doi: 10.1038/nature08655.
[40] R. Lukeman, Y.-X. Li, and L. Edelstein-Keshet, "Inferring individual rules from collective behavior," *Proc. Nat. Acad. Sci. USA*, vol. 107, no. 28, pp. 12576–12580, Jul. 2010, doi: 10.1073/pnas.1001763107.

AHMED MOREAB HUSSIEN received the B.Sc. degree in electrical engineering from the Faculty of Engineering, Future University in Egypt, Cairo, Egypt, in 2014, and the M.Sc. degree in electrical power engineering from Ain Shams University, Faculty of Engineering, Cairo, in 2021. He is currently pursuing the Ph.D. degree. He is also a LA with the Faculty of Engineering, Future University in Egypt. His research interests include power systems operation, microgrid, and renewable energy systems.

RANIA A. TURKY received the B.Sc. and M.Sc. degrees in electrical power engineering from the Faculty of Engineering, Ain Shams University, Cairo, Egypt, in 2004 and 2010, respectively. She is currently pursuing the Ph.D. degree. Her research interests include modern control techniques, power systems dynamics and control, energy storage systems, renewable energy systems, and smart grid.

ABDULAZIZ ALKUHAYLI (Member, IEEE) received the B.Sc. degree in electrical engineering from King Saud University, Riyadh, Saudi Arabia, in 2006, the M.S. degree in electrical engineering from the Missouri University of Science and Technology, Rolla, MO, USA, in 2013, and the Ph.D. degree in electrical engineering from North Carolina State University, Raleigh, NC, USA, in 2018. From 2006 to 2009, he worked as an Operation Engineer at the Energy Control Center, Saudi Electricity Company. He is currently an Assistant Professor with the Department of Electrical Engineering, King Saud University. His research interests include energy management, renewable energy systems, flexible ac transmission systems, power system stability, and smart grid.

HANY M. HASANIEN (Senior Member, IEEE) received the B.Sc., M.Sc., and Ph.D. degrees in electrical engineering from the Faculty of Engineering, Ain Shams University, Cairo, Egypt, in 1999, 2004, and 2007, respectively. From 2008 to 2011, he was a Joint Researcher with the Kitami Institute of Technology, Kitami, Japan. From 2012 to 2015, he was an Associate Professor with the College of Engineering, King Saud University, Riyadh, Saudi Arabia. He is currently a Professor at the Electrical Power and Machines Department, Faculty of Engineering, Ain Shams University. He has authored or coauthored, and edited three books in the field of electric machines and renewable energy. He has published more than 150 papers in international journals and conferences. His biography has been included in *Marquis Who's Who in the World* for its 28th edition, 2011. His research interests include modern control techniques, power systems dynamics and control, energy storage systems, renewable energy systems, and smart grid. He is an Editorial Board Member of *Electric Power Components and Systems* journal. He was awarded the Encouraging Egypt Award for Engineering Sciences in 2012, the Egypt Award for Invention and Innovation of Renewable Energy Systems Development in 2014, and the Superiority Egypt Award for Engineering Sciences in 2019. He is an IEEE PES Egypt Chapter Chair and the Editor-in-Chief of *Ain Shams Engineering Journal*. He is a Subject Editor of *IET Renewable Power Generation*, *Ain Shams Engineering Journal*, and *Electronics* (MDPI).

MARCOS TOSTADO-VÉLIZ received the B.Sc. (Hons.) and M.Sc. degrees from the University of Seville, in 2016 and 2017, respectively, and the Ph.D. degree from the University of Jaén, in 2020. He is currently an Assistant Professor at the Electrical Engineering Department, University of Jaén. His research interests include the applicability of numerical algorithms for power system analysis, energy management in microgrids, home energy management tools, and application of metaheuristic optimizers.

FRANCISCO JURADO (Senior Member, IEEE) was born in Linares, Jaén, Spain. He received the M.Sc. and Dr.Ing. degrees from the National University of Distance Education, Madrid, Spain, in 1995 and 1999, respectively. Since 1985, he has been a Professor with the Department of Electrical Engineering, University of Jaén, Jaén. His current research interests include power systems, modeling, and renewable energy.

RAMESH C. BANSAL (Senior Member, IEEE) has more than 25 years of diversified experience of research, scholarship of teaching and learning, accreditation, industrial, and academic leadership in several countries. He is currently a Professor with the Department of Electrical Engineering, University of Sharjah, and an Extraordinary Professor with the University of Pretoria (UP), South Africa. Previously, he was a Professor and the Group Head (Power) with the ECE Department, UP. Prior to his appointment at UP, he was employed with the University of Queensland, Australia; University of the South Pacific, Fiji; BITS Pilani, India; and Civil Construction Wing, All India Radio. He has significant experience of collaborating with industry and Government organizations. These utilities include NTPC (a 60 GW Indian Power Generation Company), Powerlink, and ESKOM. He has made significant contribution to the development and delivery of B.S. and M.E. programs for utilities. He has extensive experience in the design and delivery of CPD programs for professional engineers. He has carried out research and consultancy and attracted significant funding from Industry and Government Organizations. He has published over 350 journal articles, presented papers at conferences, books, and chapters in books. He has Google citations of over 12000 and H-index of 50. He has supervised 25 Ph.D., four postdoctorals, and current supervising five Ph.D. students. His research interests include renewable energy (wind, PV, microgrid), power systems, and smart grid. He is a fellow of IET, U.K., and the Institution of Engineers, India. He is an Editor/Associate Editor of several highly regarded journals, including the IEEE Systems Journal, *IET Renewable Power Generation*, and *Technology and Economics of Smart Grids and Sustainable Energy*. He is a Chartered Engineer of IET, U.K.